

14 Isotopically labeled ozone: a new approach to 15 elucidate the formation of ozonation products 16

17 Millaray Sierra Olea^a, Simon Kölle^a, Emil Bein^a, Thorsten Reemtsma^{b,c}, Oliver J.
18 Lechtenfeld^{b,d}, and Uwe Hübner^{a*}

19 ^a Chair of Urban Water Systems Engineering, Technical University of Munich, Am
20 Coulombwall 3, D-85748 Garching, Germany

21 ^b Department of Analytical Chemistry, Helmholtz Centre for Environmental Research
22 – UFZ, Permoserstrasse 15, 04318 Leipzig, Germany

23 ^c Institute of Analytical Chemistry, University of Leipzig, Linnéstrasse 3, 04103 Leipzig,
24 Germany

25 ^d ProVIS–Centre for Chemical Microscopy, Helmholtz Centre for Environmental
26 Research–UFZ, Permoserstrasse 15, 04318 Leipzig, Germany

27 * Corresponding author: Chair of Urban Water Systems Engineering, Technical
28 University of Munich, Am Coulombwall 3, D-85748 Garching, Germany

29 E-mail: u.huebner@tum.de (U. Hübner)

30 Abstract

31 As ozonation becomes a widespread treatment for removal of trace organic chemicals in
32 wastewater treatment plant effluents, there are increasing concerns regarding the
33 formation of ozonation transformation products (OPs), and their possible impacts on the
34 aquatic environment and eventually human health. In this study, a novel method was
35 developed that utilizes the heavy oxygen isotope (¹⁸O) for the production of heavy ozone
36 (¹⁸O₁O₂, ¹⁸O₂O₁, ¹⁸O₃) to actively label OPs from oxygen transfer reactions. To
37 establish and validate this new approach, venlafaxine with a well-described oxygen
38 transfer reaction (tertiary amine -> N-oxide) was chosen as a model compound. Observed
39 ¹⁸O/¹⁶O ratios in the major OP venlafaxine N-oxide (NOV) correlated with expected ¹⁸O
40 purities based on previous tracer experiments. These results confirmed the successful
41 labeling with heavy oxygen and furthermore demonstrate the potential to monitor NOV as
42 an indicator of ¹⁸O/¹⁶O ratios during ozonation. As a next step, ¹⁸O/¹⁶O ratios were used
43 to elucidate the formation mechanism of previously described OPs from
44 sulfamethoxazole (SMX). Seven OPs were detected including the frequently described
45 nitro-SMX, which was formed with a maximum yield of 3.2% (of initial SMX). With the
46 successful labeling of six of the seven OPs from sulfamethoxazole, it was possible to
47 confirm their previously proposed formation pathways, and distinguish oxygen transfer

48 from electron transfer reactions. OPs $^{18}\text{O}/^{16}\text{O}$ ratios indicate that hydroxylation of the
49 aromatic ring and formation of nitro-groups mostly follows oxygen transfer reactions, while
50 electron transfer reactions initiate the formation of hydroxylamine and the abstraction of
51 NH_2 leading to catechol.

52 **Keywords: ozonation products, oxygen-18, isotope labeling,**
53 **wastewater**

54 1. Introduction

55 Chemicals of Emerging Concern (CECs) have their origin in our daily domestic and
56 industrial applications (Loos et al., 2013; Margot et al., 2013). The main concern with
57 CECs is related to their biologically active design and wide range of application (Lee
58 and Von Gunten, 2016). Their high polarity and poor degradability (high persistence)
59 prevents the efficient removal in conventional WWTPs (Reemtsma et al., 2006), which
60 results in constant discharge into surface waters at detectable concentrations (ng L^{-1}
61 to $\mu\text{g L}^{-1}$) (Margot et al., 2013; Ternes et al., 2003). Ozonation is an advanced treatment
62 technology currently used in wastewater treatment plants (WWTPs) to reduce the
63 concentrations of CECs in their discharged effluent (Bourgin et al., 2018; Eggen et al.,
64 2014; Gulde et al., 2021; Huber et al., 2005; Margot et al., 2013; Ternes et al., 2003).
65 Despite the known benefits of ozone for oxidation, which often leads to immediate loss
66 of biological activity (e.g., hormones, antibiotics) (Huber et al., 2004) there are still
67 uncertainties regarding the transformation of CECs into a mix of unknown and
68 potentially hazardous ozonation products (OPs) (Hübner et al., 2015; Lee and Von
69 Gunten, 2016; Wert et al., 2007).

70 OPs are formed by the partial oxidation of compounds when they react with ozone (von
71 Gunten, 2003; Von Sonntag and Von Gunten, 2012). The selective reaction of ozone
72 often results in a limited number of major OPs (Lim et al., 2019; Zucker et al., 2018),
73 with their formation controlled by the reactive functional groups in the parent compound
74 (Tentscher et al., 2019). In contrast, diffusion dependent reactions with hydroxyl
75 radicals ($\bullet\text{OH}$), that are generated as secondary oxidants from ozone reactions with
76 the water matrix, form numerous OPs at low individual concentration (von Gunten,
77 2003).

78 With the current understanding of ozone reaction mechanisms, examples of OPs
79 formation from parent functional groups, are: N-oxides and dealkylated products
80 formed from tertiary amines, nitroalkanes and or hydroxylamines formed from aliphatic
81 primary and secondary amines, hydroxylated compounds formed from aromatic
82 scaffolds, as well as, aldehydes and ketones formed from unsaturated carbons chains
83 (Lee and Von Gunten, 2016; Lim et al., 2019; Tekle-Röttering et al., 2016; Zucker et
84 al., 2018). Knowledge gaps still exist for ozonation reaction kinetics and mechanisms
85 for Sulfur (S) and Nitrogen (N) containing moieties. In S- containing moieties (thiols,
86 thioethers, and disulfides), the formation of a sulfoxide (SO) has been proposed as the
87 most common functional group (Dodd et al., 2010), but only limited knowledge about
88 the possible subsequent reactions to form sulfone (SO₂), sulfonic acid (SO₃H), and
89 sulfate (SO₄²⁻) is available (Lim et al., 2022). For N- containing moieties, there is
90 uncertainty in the case of secondary amines, where, although hydroxylamines were
91 suggested as a major product, studies have shown that this might be only an
92 intermediate and nitro-alkanes are the major OP (Lim et al., 2022).

93 In previous experiments focused on drinking water treatment, the use of isotopically
94 labeled (¹³C, ¹⁵N and ²H) parent compounds facilitated the identification of reaction
95 sites for ozone, as well as, the elucidation of the formed OPs by their characteristic
96 isotopic pattern (Brunner et al., 2019; Kolkman et al., 2015; Liu et al., 2019; Spahr et
97 al., 2015; Spahr et al., 2017). The use of labeled compounds (¹³C, ¹⁴C, ¹⁵N and ²H)
98 has also been applied to study different CECs and their OPs kinetics and formation
99 pathways in WWTP (Betsholtz et al., 2022; Borowska et al., 2016; Dodd and Huang,
100 2004; Mawhinney et al., 2012; Willach et al., 2017). These studies have focused on
101 particular compounds considered relevant, either by their abundance or by their
102 toxicity, but were not based on the reactivity of the specific functional groups with
103 ozone. Because of the overwhelming number of CECs and organic matter in
104 wastewater, rather than evaluating every single compound and its OPs in a complex
105 mixture, it is more efficient to generate transferable knowledge regarding individual
106 functional group reactivity with ozone and the expected OPs (von Gunten, 2018).

107 The objective of this study is to establish and validate a novel isotope labeling method
108 by using isotopically labeled ozone ([¹⁸O]₃) to oxidize selected model compounds and
109 produce isotopically labeled OPs. The method has been validated by the ozonation of
110 a model substance (Venlafaxine) with well-known reaction mechanism with ozone
111 (tertiary amine -> N-oxide), and then applied to investigate the reaction mechanism of

112 sulfamethoxazole (sulfonamide) leading to formation of 4-nitro-sulfamethoxazole and
113 other OPs. By using this approach, we put emphasis on functional group reactivity
114 towards ozone. This alternative approach can supply information such as reaction
115 site/preference when more than one functional group is present, explicit reaction
116 mechanism and reaction pathway for OPs formation, and enable the detection of OPs
117 and ozonation by-products (OBPs) formed during ozonation of complex wastewater or
118 drinking water matrices. In a parallel study, we successfully implemented our new
119 concept for the detection of OBPs during the ozonation of effluent organic matter
120 (EfOM) (Jennings et al., under review). The results from this study demonstrate that
121 labeling of the OPs allows extrapolation of knowledge to more complex scenarios.

122 2. Materials and Methods

123 2.1. Chemicals and reagents

124 For sample preparation, the following compounds were used: venlafaxine
125 hydrochloride (VLX), sulfamethoxazole (SMX) primidone (PRI), and tert-butanol (t-
126 BuOH, ≥99 %). Technical O₂ and N₂ gases were used for initial testing of the system.
127 Heavy oxygen gas (¹⁸O₂ ≥97%) was used for the production of labeled ozone.
128 Additional information regarding the chemicals and gases used can be found in the SI,
129 Table S 1.

130 2.2. Generation of labeled ozone stock solution

131 *Configuration of the ozonation system.* A previously established ozonation system
132 (Müller et al., 2019) was modified with the addition of two gas feedlines (¹⁸O₂, N₂) and
133 the positioning of 2- and 3-way valves (SI, Figure S 1). These modifications allow the
134 system to be operated as a closed-circuit with the possibility of recovering the used
135 gas from the experiments. A bellows pump (5 NL min⁻¹) was used to maintain and
136 guarantee the gas flow inside the system. For gas conditioning, two water traps with
137 molecular sieve 3 Å were placed before the ozone generator. The reactor volume was
138 500 mL and a needle valve port was implemented for the controlled extraction of the
139 ozone stock solution. For additional information regarding the components of the
140 system, refer to SI Table S 2.

141 *Determination of mixing ratios using N₂ and O₂ gases.* To simulate mixing and
142 concentration of gases, tracer tests with N₂ and O₂ gases were conducted to determine
143 optimum times for operating (opening and closing) of the gas lines, as well as,
144 establishing the optimal conditions of gas pressure and flow. The test was performed
145 by initially saturating the system with 100% O₂ gas until stable reading in an inline
146 oxygen sensor. Subsequently, the two valves controlling O₂ and N₂ were
147 simultaneously closed and opened, respectively. Finally, after a pre-determined
148 amount of time, the valve controlling the system mode (open circuit vs. gas
149 recirculation) was closed. The breakthrough curves obtained from the shift from
150 100 % O₂ to N₂ as well as the final mixing ratios were monitored in the inline oxygen
151 sensor.

152 *Generation of the ozone solution.* Technical O₂ gas and ¹⁸O₂ (≥97%) gas were used
153 as input-gas for the ozone generator BMT 803 BT. The ozone gas was continuously
154 bubbled in the reactor, which was filled with ultrapure water and cooled in an ice-filled
155 container (~4°C). Required volumes of ozone stock solution (to set a concentration of
156 approximately 25 mg L⁻¹) were extracted from the reactor using a gastight glass
157 syringe. This volume was used to determine the dissolved ozone concentration in the
158 stock solution and for the ozonation of the samples. The dissolved ozone concentration
159 was measured by the colorimetric indigo carmine method (Bader, 1982).

160 2.3. Batch ozonation experiments

161 *Sample preparation.* Samples for batch experiments with VLX and VLX/SMX were
162 prepared in separate 20 mL vials. To elucidate the reaction mechanism of ozone with
163 model compounds, the formed hydroxyl radicals (•OH) were scavenged by using t-
164 BuOH with a k_{OH} 6 x 10⁸ M⁻¹ s⁻¹ (Von Sonntag and Von Gunten, 2012). The necessary
165 concentrations of t-BuOH for the experiments with VLX and VLX/SMX were adjusted
166 according to Willach et al. (2017). To corroborate the efficiency of the scavenging
167 agent, primidone with a k_{O_3} 1 M⁻¹ s⁻¹ and k_{OH} 6.7 x 10⁹ M⁻¹ s⁻¹ (Real et al., 2009) was
168 used as a radical indicator. In parallel, samples without t-BuOH were prepared. All
169 samples for ozonation were prepared in phosphate buffer at pH 7. A detailed
170 composition for each batch experiment is given in SI, Table S 3.

171 *Ozonation experiments.* To establish the labeling method and validate its performance,
172 initial experiments with VLX as sole ozone reactive compound were performed. As

173 reported by Zucker et al. (2018), the major ozonation product of venlafaxine is
174 venlafaxine-N-oxide (NOV). The reaction mechanism of this compound proceeds by
175 the transfer of one oxygen atom from the ozone molecule to the nitrogen of the tertiary
176 amine functional group (SI, Figure S 3). Alternative transformation reactions (i.e., N-
177 dealkylation, ozone attack at the activated aromatic ring) were not considered since
178 they were only expected to affect the yield of NOV but not its $^{18}\text{O}/^{16}\text{O}$ ratio.

179 Consequently, a total of six experiments were performed. Three experiments were
180 completed with VLX as sole reactive compound: first with technical ^{16}O gas, and two
181 experiments with the different times previously characterized for the change of the gas
182 lines at 0.5 bar (9 sec and 17 sec). In these batch experiments $20\ \mu\text{mol L}^{-1}$ of VLX was
183 oxidized using ozone dosages of $20 - 100\ \mu\text{mol L}^{-1}$. Subsequently, three additional
184 experiments were performed at 0.9 bar with adjusted times for the gas line change
185 according to breakthrough curves experiments (13 sec and 21 sec). One experiment
186 was of VLX as sole reactive to corroborate the impact of pressure in the expected ^{18}O
187 purity. The approach of labeling of OPs with ^{18}O was then applied to investigate
188 transformation reactions for SMX. Samples containing a 1:5 molar ratio of VLX/SMX
189 ($10\ \mu\text{mol L}^{-1}$ VLX, and $50\ \mu\text{mol L}^{-1}$ SMX) were prepared and oxidized with ozone
190 dosages of $50 - 300\ \mu\text{mol L}^{-1}$. A list of the targeted molar ratios for both compounds
191 can be found in SI, Table S 4. The volume in all experiments was adjusted to 10 mL
192 and samples were stored at 4°C until measurement.

193 2.4. Sample analysis

194 *Compound quantification.* Samples were measured on an LC-MS/MS (PLATINblue
195 UHPLC – Knauer, Germany, ABSciex TQUAD 6500 – SCIEX, USA), using a method
196 established and described by Müller et al. (2017). Quantification of VLX, venlafaxine
197 N-oxide (NOV), SMX and PRI was accomplished in positive MRM (multiple reaction
198 monitoring) mode. The quantification of the OPs 4-nitro sulfamethoxazole (NIT), was
199 performed in negative MRM mode. To determine the $^{18}\text{O}/^{16}\text{O}$ ratio in labeled NOV and
200 NIT, the qualifying and quantifying fragments' m/z values were modified to include the
201 expected labeling site and mass shift. For additional information regarding Q1 and Q3
202 masses and internal standards, refer to SI, Table S 5.

203 *Separation and detection of SMX OPs.* The separation of the OPs from SMX was
204 performed with a Waters XSelect HSS T3 column (100\AA , $3.5\ \mu\text{m}$, $2.1\ \text{mm} \times 100\ \text{mm}$,

205 Waters Germany) on an LC-MS system (Agilent 1260 Infinity – Agilent Technologies,
206 USA, ABSciex Qtrap 5500 - SCIEX, USA). For the separation of the compounds, a
207 gradient method was developed (SI, Table S 6). The solvents used were, ultrapure
208 water (Arium Pro, Sartorius AG, Göttingen, Germany) and acetonitrile (hypergrade for
209 LC-MS, LiChrosolv, Merck KGaA, Darmstadt, Germany) supplemented with 0.1%
210 formic acid (LC-MS grade, HiPerSolv, VWR Chemicals, Leuven, Belgium). For
211 compound detection in negative mode, Enhanced MS Scan (EMS) and Enhanced
212 Product Ion Scan (EPI) were applied. The mass ranges used in both scan types can
213 be found in SI, Table S 7. Data exploration and integration of the peak areas was
214 performed with the software Analyst 1.6.2 (ABSciex - SCIEX, USA).

215 2.5. Data handling and calculations

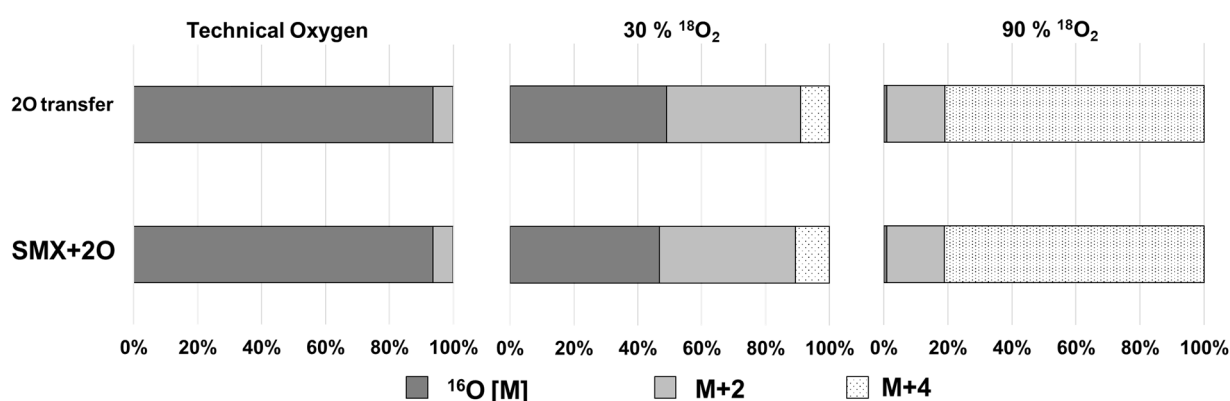
216 *Analysis of SMX OPs.* For the integration of peak areas of the labeled SMX OPs,
217 isotopologue fractions (IF) for the monoisotopic mass and the integration of up to two
218 labeled oxygen atoms were determined according to Mairinger and Hann (2020). The
219 MS¹ scans of individual samples and their isotopologue peaks were analyzed focusing
220 on their centroid mass (Da), peak start (Da) and peak end (Da). Mean and standard
221 deviation of discrete *m/z* ranges were used to define the starting and ending values for
222 the different isotopic distribution of the isotopologues (SI, Table S 8). Once discrete
223 and nonoverlapping *m/z* ranges were determined, isotopologue peak areas with M+0
224 ([¹⁶O], 2[¹⁶O]), M+2 Da ([¹⁸O]) and M+4 Da (2[¹⁸O]) were integrated (SI, Table S 9). It
225 should be noted that these calculations were performed by evaluating MS¹ data with
226 low resolution.

227 *Oxygen transfer reaction probabilities.* The ¹⁸O/¹⁶O ratios determined in the formed
228 NOV (from single oxygen transfer reaction to VLX) were applied to elucidate the
229 formation pathway of OPs from SMX. These ¹⁸O/¹⁶O ratios were used to calculate the
230 expected isotopologue fractions during the formation of SMX OPs with two oxygen
231 additions (eq. 1), where *x* and *y* denote the number of ¹⁶O and ¹⁸O atoms and Pr(¹⁶O)
232 and Pr(¹⁸O) represent the probabilities determined by VLX measurements (modified
233 from Valkenburg et al. (2012)).

$$234 \quad Pr(^{16}O_x ^{18}O_y) = \frac{(x+y)!}{x! \times y!} Pr(^{16}O)^x \times Pr(^{18}O)^y \quad (1)$$

235 However, this calculated isotopologue distribution does not yet consider the natural
236 isotopologues of the parent molecule. The web platform *enviPat* (Loos et al., 2015)

237 was used to predict the expected isotopic pattern of SMX + 2O, and the relative
 238 abundance of relevant natural isotopologues (monoisotopic mass [M], M+2) (SI, Text
 239 S 1). As an example, the calculated distribution of SMX-OPs with and without
 240 consideration of natural isotopologues are illustrated in Figure 1 for assumed
 241 probabilities of ^{18}O ($\text{Pr}(^{18}\text{O})$) of 0%, 30% and 90%. Results indicate a limited effect of
 242 the natural isotopologues on the distribution of ^{18}O -OPs from SMX, but this might
 243 become different for ozonation of larger molecules, especially when they contain
 244 several sulfur atoms. These hypothetical values were then contrasted with the
 245 empirical results obtained from signal intensities of SMX OPs.



246
 247 Figure 1. Example calculation of the expected isotopologue fractions (IF) of an SMX-
 248 OPs from two oxygen transfer reactions with and without consideration of relevant
 249 natural isotopologues (^{13}C , ^{15}N , ^{33}S , ^{34}S , ^{36}S , ^{17}O , ^{18}O) from SMX. Results show
 250 hypothetical distributions for ozonation with ozone from technical oxygen (^{16}O), 30%
 251 ^{18}O and 90% ^{18}O .

252 3. Results and Discussion

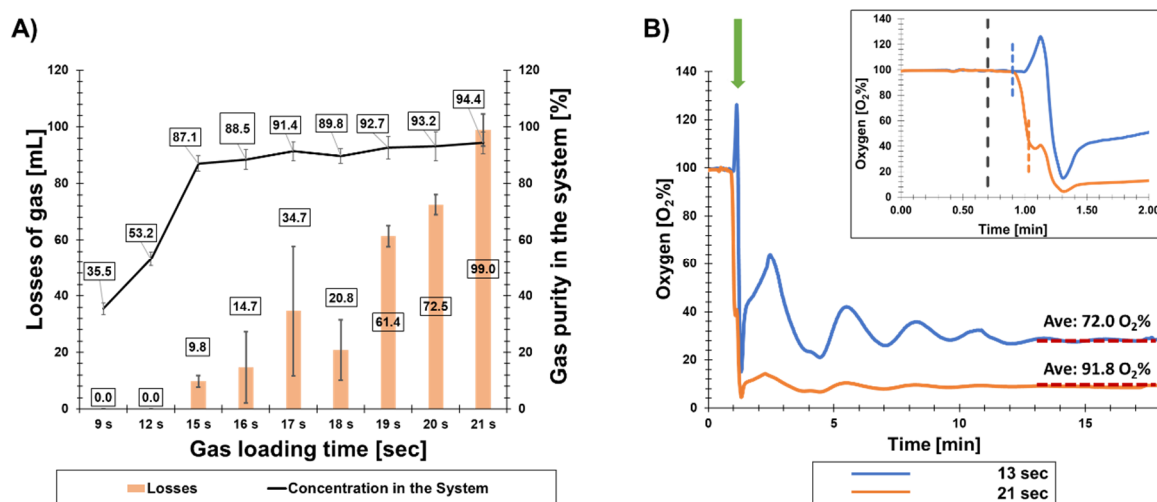
253 3.1. Method development and validation

254 The establishment and validation of the novel labeling method was performed as
 255 follows: (1) evaluation of N_2 and O_2 gas mixing ratios, (2) quantification of the $^{18}\text{O}/^{16}\text{O}$
 256 ratio in NOV, and (3) correlation of the gas mixing ratios with labeling success of NOV.
 257 Following this approach, we were able to confirm the suitability of VLX to indicate the
 258 $^{18}\text{O}/^{16}\text{O}$ of OPs from oxygen transfer reactions.

259 *Determination of mixing ratios using N_2 and O_2 gases.* The purity of $^{18}\text{O}_2$ depends on
 260 the gas loading time (seconds), which is the duration of gas feeding from the $^{18}\text{O}_2$
 261 container before the ozonation system is changed to recirculation mode. We simulated

262 $^{18}\text{O}_2$ purity by exchanging O_2 with N_2 . Initially, nine different gas loading times were
 263 tested during operation at 0.5 bar generator pressure in replicate experiments
 264 (minimum 2 to up to 17 replicates for most promising settings) and gas loading times
 265 were compared with regards to their mixing ratios (simulated purity of $^{18}\text{O}_2$), and the
 266 volume of gas that could not be recovered for future experiments (Figure 2A). Since
 267 an increase in gas loading times beyond 17 s did not considerably improve gas purity
 268 to values $>90\%$, this operational setting was selected for experiment with highest
 269 purity of labeled ozone production (91.4%). In addition, experiments with 9 s were
 270 conducted to obtain the lowest purity of $^{18}\text{O}_2$.

271 After slight modifications of the ozone system (increased volume from additional
 272 dehumidification, higher generator pressure of 0.9 bar), experiments were repeated
 273 with slightly different gas loading times of 13 s and 21 s. Two example breakthrough
 274 curves are shown in Figure 2B. Results demonstrate that full breakthrough is reached
 275 after approximately 30 - 40 s, followed by several minutes of oscillation in the
 276 recirculated system until both gases are fully mixed. In addition, the green arrow in
 277 Figure 2B demonstrates the impact of pressure on the oxygen sensor, as the 20%
 278 increase in O_2 gas can only be explained by a pressure change in the system after
 279 switching from gas feeding to recirculation (see SI, Text S 2 for details). Also the type
 280 of gas being exchanged (O_2 to N_2 vs N_2 to O_2) seems to affect the results (SI, Figure
 281 S 2).



282

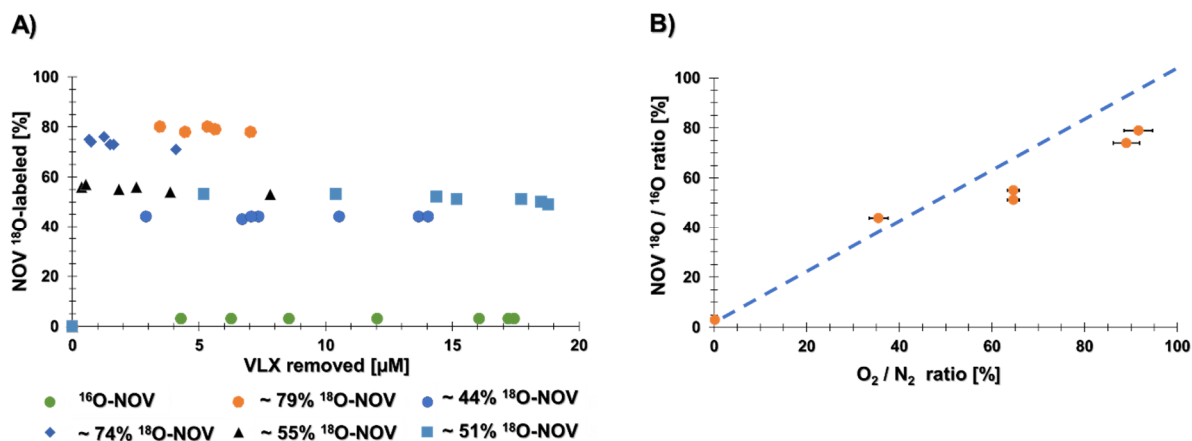
283 Figure 2. **(A)** The purity of $^{18}\text{O}_2$ that is expected depending on the gas loading times,
 284 as well as, the volume of gas that would be purged in each of the tested times. Error
 285 bars indicate standard deviation from variable number of replicates (2 - 27) at different
 286 times. **(B)** Breakthrough curve observed in the experiments for determination of system

287 settings and $^{18}\text{O}_2$ purity determination. The inlet shows the first 2 min with the dotted
288 black line indicating the change of gas lines, the dotted blue and orange lines the times
289 the system was closed.

290 *Determination of $^{18}\text{O}/^{16}\text{O}$ ratios using NOV.* With the operational protocol established,
291 the expected ^{18}O gas purity simulated with the tracer N_2/O_2 experiments were
292 corroborated by performing heavy ozone experiments and using the ozonation product
293 NOV of VLX as indicator of labeling success. As a reference for the isotope distribution
294 of OP formed by ozonation, the relative ion intensity of NOV in an experiment with $^{16}\text{O}_3$
295 was quantified (97 % m/z 294 $[\text{M}+\text{H}]^+$ and 3 % m/z 296 $[\text{M}+\text{H}]^+$). This isotope pattern
296 was additionally compared with the values obtained from the calculation performed by
297 using the *enviPat* platform (Loos et al., 2015) (SI, Text S 3). Because these samples
298 were analyzed with an MRM method, with modified Q1 and Q3 masses that considered
299 the labeled fragment, other possible isotopologues were not measured.

300 In the ozonation experiments with different $^{18}\text{O}/^{16}\text{O}$ ratios, the oxygen transfer reaction
301 was confirmed by the changes in the relative abundance of the isotopic fraction of the
302 detected peaks ($[\text{M}+0]$, $[\text{M}+2]$) of the produced NOV molecule (Figure 3A). Therefore,
303 when comparing the values for m/z 294 $[\text{M}+\text{H}]^+$ and m/z 296 $[\text{M}+\text{H}]^+$ obtained in the
304 $^{16}\text{O}_3$ experiments, with the results observed in the produced NOV m/z of the different
305 $^{18}\text{O}/^{16}\text{O}$ ozone experiments, the labeling success was reflected in the results, where
306 the highest labeling success was $79 \pm 1\%$ ^{18}O -NOV, meanwhile the lowest was
307 $43.9 \pm 0.3\%$ ^{18}O -NOV. The results of these experiments show that the $^{18}\text{O}/^{16}\text{O}$ ratios
308 of the labeled NOV are stable and independent of the removed VLX, and ozone
309 concentration dosed.

310 Additionally, as shown in Figure 3B, the $^{18}\text{O}/^{16}\text{O}$ ratio of labeled NOV changed
311 according to the simulated concentrations of $^{18}\text{O}_2$ (O_2/N_2 ratio) in the system.
312 Increasing the proportion of heavy oxygen in the ozonation system, increased the
313 proportion of the heavy-labeled transformation product (^{18}O -NOV). The correlation
314 between both variables was found to be $R^2 = 0.9605$, which indicates that ^{18}O -NOV
315 formation is a suitable proxy for the estimation of the $^{18}\text{O}/^{16}\text{O}$ ratio.



316

317 Figure 3. (A) Labeling of NOVA depending on the $^{18}\text{O}/^{16}\text{O}$ ratios applied in the ozonation
 318 experiments with different ^{18}O purities (B) the relative intensity of the ions of interest
 319 for the experiments with a range of different $^{18}\text{O}_3 / ^{16}\text{O}_3$ concentrations compared to
 320 expected ratios from N_2/O_2 experiments.

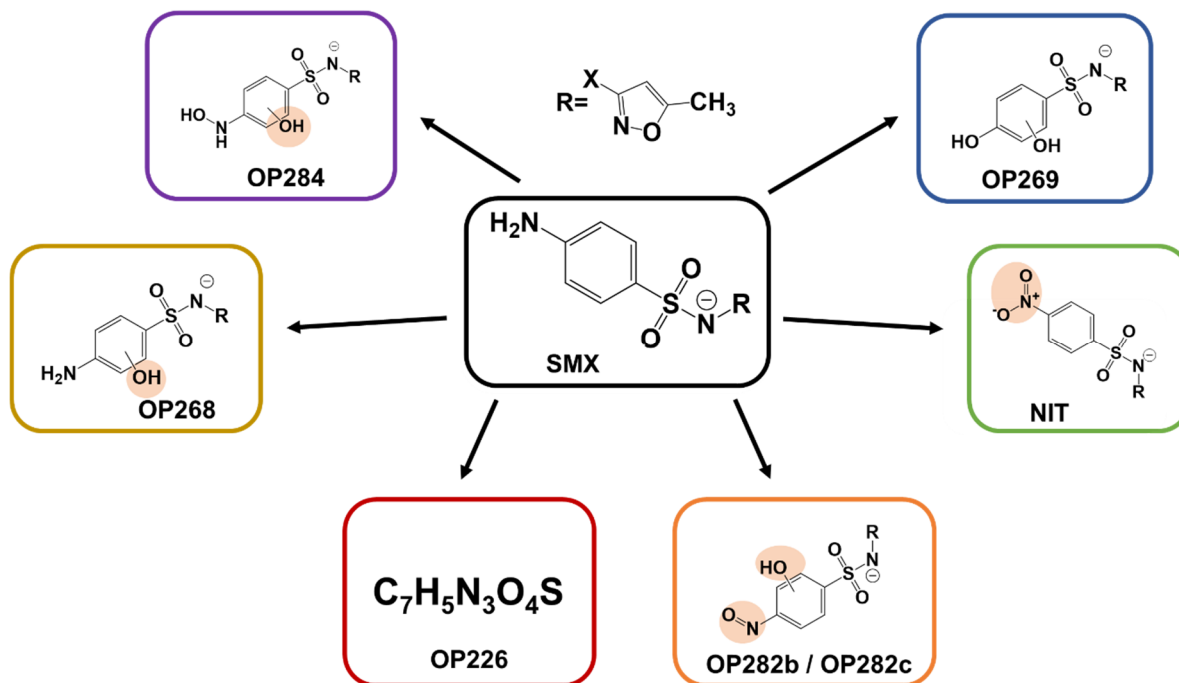
321 However, as can be seen in Figure 3B the labeling success has an observable
 322 scattering that can be explained by different factors. First, the system is operated by a
 323 human and the changing of the gas lines must be done in seconds, thus any
 324 millisecond delay or mistake will considerably impact the gas purity. Second, the
 325 estimation of the oxygen percentage depends on the pressure in the gas line (see
 326 Figure 2A), therefore a higher reading of the oxygen sensor should be taken into
 327 consideration. Third, two different purities of $^{18}\text{O}_2$ were used for the production of
 328 ozone, the first had a purity of 99 $^{18}\text{O}\%$ (Sigma-Aldrich, USA), the second 97 $^{18}\text{O}\%$
 329 (Linde GmbH, Germany). Fourth, the isotope kinetic effect of the four possible
 330 isotopologues of ozone is unknown, indicating some uncertainty regarding their
 331 individual reaction rates with VLX. Notwithstanding, the changes in the isotopic pattern,
 332 the formed NOVA is produced by the change in the abundance of ^{16}O and ^{18}O in the
 333 system and the labeling of this compound with ^{18}O will therefore be used as a surrogate
 334 to establish $^{18}\text{O}/^{16}\text{O}$ ratios during following experiments with other compounds and
 335 matrices.

336 3.2. Sulfamethoxazole pathway elucidation

337 *Quantification and semi-quantification of SMX OPs.* In experiments with ^{16}O -ozone, six
 338 OPs were separated and detected (Figure 4). These products were previously reported
 339 in other studies, providing MS data and possible formation pathways (Gao et al., 2014;

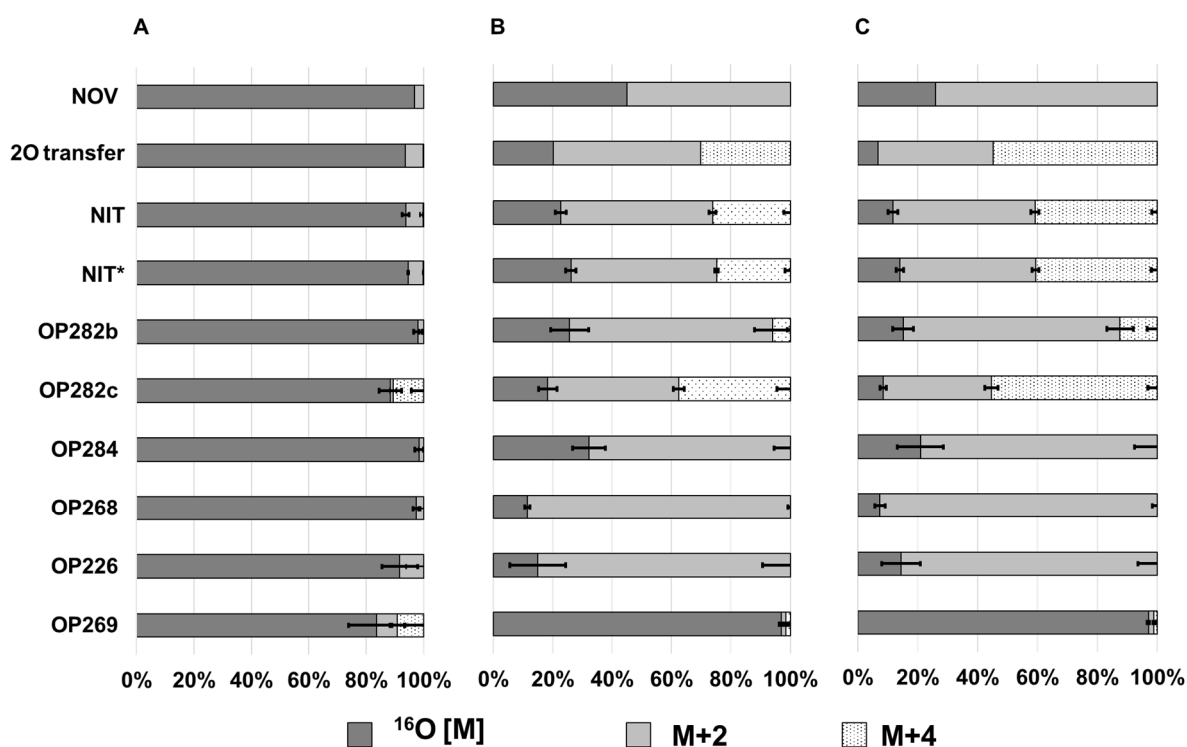
340 Gómez-Ramos et al., 2011; Willach et al., 2017). Additionally, it was possible to detect
 341 a seventh previously unreported OP, OP284. To confirm the chemical identity of
 342 OP282a, the commercially available standard for 4-nitro-sulfamethoxazole (NIT) was
 343 used, this also enabled its quantification (SI, Figure S 5). The yield of NIT produced
 344 was $3.2 \pm 0.3 \%$ when the removal of SMX was $99.8 \pm 0.2 \%$ (SI, Figure S 6). These
 345 values are within the previously 10% reported by Tekle-Röttering et al. (2016) for total
 346 product yield of nitrobenzene, nitrosobenzene and azobenzene, although in our work
 347 it was not possible to detect the formation of nitroso or azo sulfamethoxazole OPs.
 348 Additionally, there was no significant difference in the removal of SMX and the
 349 formation of labeled NIT, regardless of the $^{18}\text{O}/^{16}\text{O}$ ratio used for the production of the
 350 labeled ozone.

351 Peak areas (counts) of the seven OPs can be found in SI, Figure S 7. There, the
 352 formation of the OPs is illustrated as a function of the SMX removal. The comparison
 353 of cumulative intensities from isotopologues (IF) with results from ozonation with
 354 technical oxygen does not show any systematic deviation that would indicate different
 355 behavior of ozonation with different $^{18}\text{O}_2$ abundances.



356
 357 Figure 4. Detected OPs from SMX with proposed structures assigned based on
 358 previous studies (orange circles highlight the formed functional group with oxygen-18
 359 added to the molecule, numbers indicate m/z in negative mode).

360 *Application of $^{18}\text{O}/^{16}\text{O}$ ratios in VLX/SMX ozonation.* Figure 5 illustrates measured
 361 isotopologue distributions for all detected SMX-OPs in comparison to the expected
 362 distribution for transfer of one oxygen (indicated by NOV distribution) and the expected
 363 probabilities for two oxygen transfer reactions (shown as 2O transfer).



364

365 Figure 5. Change of the isotopologue distribution in the formation of different SMX
 366 OPs. OPs obtained from ozonation with technical oxygen (A) are compared to OPs
 367 obtained from ozone with a $55 \pm 1.5\%$ ^{18}O purity (B) and $74 \pm 1.3\%$ ^{18}O purity (C)
 368 based on NOV measurements (NIT* was quantified by MRM using the transitions m/z
 369 282/186, m/z 284/188 and m/z 286/190, while all other isotopologue distributions were
 370 derived from the intensity of the respective molecular ions). Error bars indicate
 371 standard deviation observed in the formation of labeled OPs being produced by
 372 different ozone dosages.

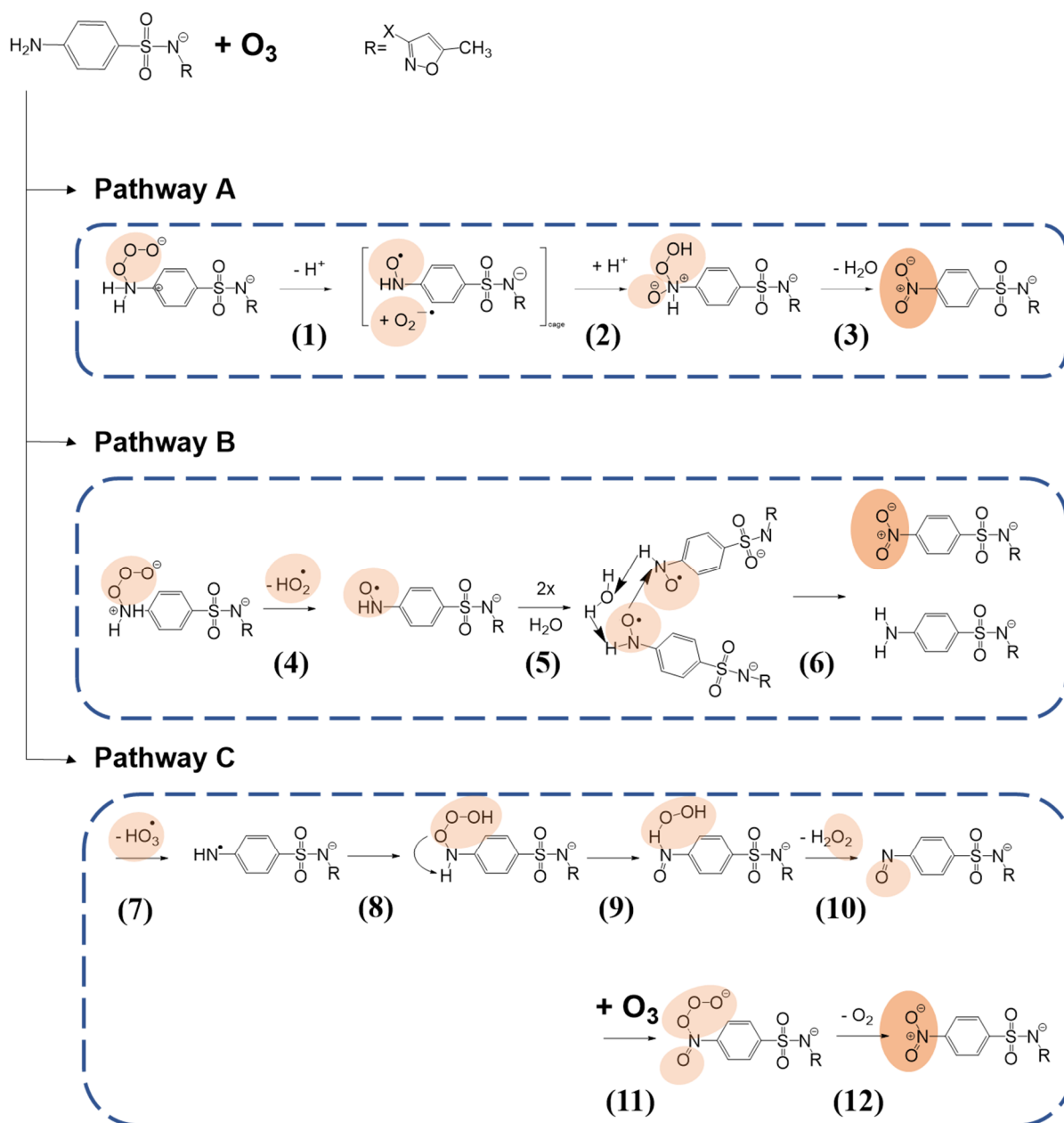
373 Six of the seven detected OPs from SMX showed a shift in their monoisotopic peak
 374 area and isotopologue fraction, aligning with the measured NOV $^{18}\text{O}/^{16}\text{O}$ ratio. These
 375 shifts in the isotopic pattern of the ion indicate the successful addition of one or two
 376 ^{18}O atoms during ozonation. As can be seen in Figure 5, the three isomers of m/z 282
 377 (NIT, OP282b and OP282c) seemed to be a result of two oxygen transfer reactions
 378 from the labeled ozone. Isotopologue distributions of NIT were determined from
 379 integration of qualitative MS¹ data (shown as NIT) and from MRM quantification (NIT*).
 380 Overall, results show a good agreement between both analytical methods, indicating

381 that MS¹ data is suitable to assess isotopologue distribution for other OPs without an
382 available standard. Minor differences, although significant (p -value < 0.05) when
383 comparing between the measurements of the isotopologues fractions of NIT (m/z 282,
384 284 and 286) and the results obtained from the integration of the fragments of interest
385 in (OP282NIT*) (m/z 282/186, m/z 284/188 and m/z 286/190 of the 55 %¹⁸O₂), can be
386 explained by the higher selectivity of the MRM method and the different criteria used
387 for the data integration. OPs 282b and 282c showed stronger deviation from expected
388 distribution for 2O transfer reactions. Occurrence of the m/z 286 isotopologue of
389 OP282c after ozonation with ¹⁶O₃ indicates co-elution of a different molecule at the
390 same retention time, which can explain the shift in all experiments. In contrast, limited
391 formation of m/z 286 for OP282b might be related to competing reactions of the
392 intermediate, e.g. parallel oxidation by ozone and dissolved oxygen.

393 The formation of OP284, OP268, and OP226 can be explained by one oxygen transfer
394 reaction (Figure 5). The observed deviation in their ¹⁸O content from the value
395 expected from NOV may be due to their low peak areas. While OP268 and OP226 are
396 solely generated through oxygen transfer reaction, OP284 contains an additional
397 oxygen, which was not derived from ozone. Lastly, OP269 is the single OP not being
398 formed by a direct oxygen transfer reaction from the labeled ozone despite the addition
399 of 2 oxygen atoms during the reaction. The direct reaction of O₃ with the aromatic ring
400 or nitrogen functional group has been proposed as formation pathway for several of
401 the reported OPs of SMX (Gao et al., 2014; Gómez-Ramos et al., 2011; Willach et al.,
402 2017). However, the ¹⁸O-labelling approach developed in this study is the first to prove
403 the origin of the oxygen in the ozonation products. This illustrates how ¹⁸O-labeling
404 gives additional insight into the mechanism and transformation pathways during
405 ozonation.

406 *Elucidation of ozone reaction pathways.* For the formation of NIT, two different
407 formation pathways were proposed by Willach et al. (2017). Pathway A (reaction (1)-
408 (3)) in Figure 6 was proposed based on the reaction of ozone as an H-abstractor with
409 the formation of a radical pair, a subsequent cage reaction and release of water (Tekle-
410 Röttering et al., 2016). Pathway B (reaction (4)-(6)) was proposed based on the
411 insertion reaction of ozone at the nitrogen, where the intermediate would release a
412 hydroperoxyl radical and form a nitroxyl radical, which would decay assisted by water
413 once again forming sulfamethoxazole and 4-nitro sulfamethoxazole (Von Sonntag and
414 Von Gunten, 2012). A third alternative, formation pathway C, was proposed by Yu et

415 al. (2017) by using density functional theory (DFT). They proposed a hydrogen atom
 416 transfer (HAT) mechanism as the first step, producing an amino radical and a $\bullet\text{OOH}$
 417 radical, which would recombine with the amino radical. This newly formed intermediate
 418 could have its H_2O_2 replaced by ozone, releasing O_2 and forming the nitro group
 419 (reaction (7)-(12)). These three previously proposed pathways have in common that
 420 the two transferred oxygen atoms originate from the ozone molecule. This agrees with
 421 the results obtained from the labeling experiments, where both transferred oxygen
 422 atoms are labeled according to the expected $^{18}\text{O}/^{16}\text{O}$ ratios. Therefore, it is not possible
 423 to distinguish based on probabilities, which one of these three pathways (Figure 6) is
 424 responsible for the formation of the nitro group.



425

426 Figure 6. Three proposed formation pathway for the formation of 4-nitro-

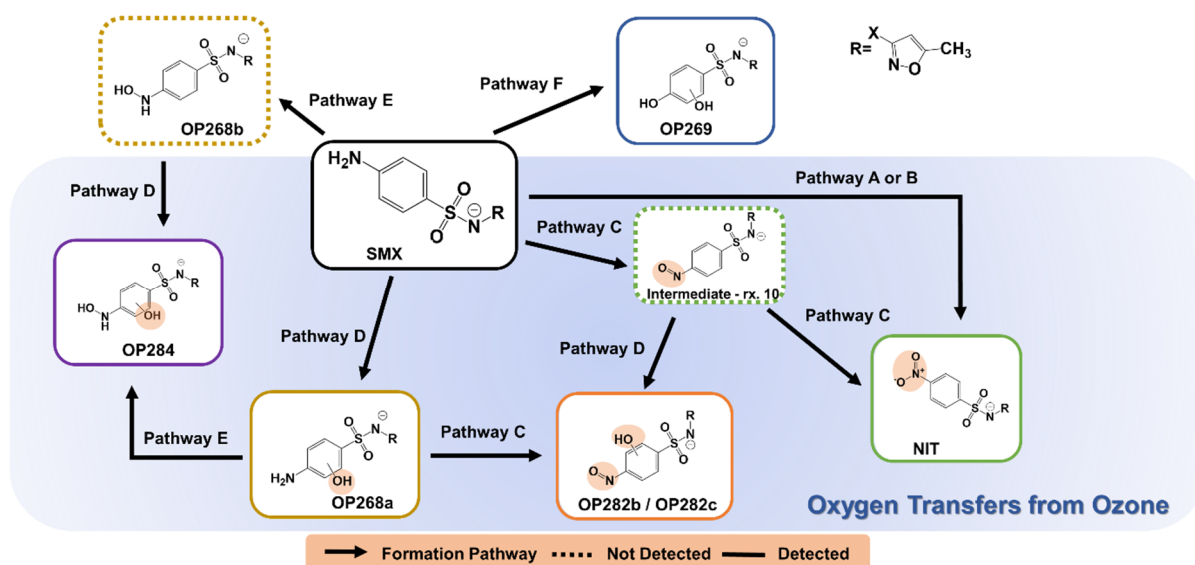
427 sulfamethoxazole (Extracted Willach et al. (2017) and Yu et al. (2017)). Orange circles
428 highlight the presence of ^{18}O .

429 ^{18}O labels in the proposed hydroxylated structures OP282b/c and OP268 indicate that
430 hydroxylation predominately follows an oxygen transfer (addition) reaction as
431 described by Tekle-Röttering et al. (2016) for aniline. In the case of OP268, a single
432 hydroxylated OP, it was not possible to separate the two isomers described by Willach
433 et al. (2017). In their study, they confirmed that one of these isomers was
434 sulfamethoxazole hydroxylamine (OP268b), which can imply that the other detected
435 isomer of OP268 (OP268a) could be formed by the reaction of ozone with the aromatic
436 ring (SI, Figure S 8, pathway D). They proposed a formation pathway starting with an
437 H-abstraction from the anilinic nitrogen leading to the formation of an aminyl radical
438 (Yu et al., 2017). This aminyl radical would then react with oxygen to form a peroxy
439 radical, which would imply the reaction of two peroxy radicals, and their decay via the
440 Russell mechanism to finally form the hydroxylamine (SI, Figure S 8, pathway E). In
441 this formation pathway the transferred oxygen atom has its origin in the reaction of the
442 aminyl radical with an oxygen molecule, which is contradicted by the observed shift in
443 the isotope pattern of the formed OP268 (see Figure 5). Therefore, the formation
444 pathway for the detected OP268a is better described by the transfer of an oxygen atom
445 from the ozone molecule (Figure 7), although the precise location of the labeled oxygen
446 could not be distinguished between the aromatic ring or the nitrogen moiety.

447 Gómez-Ramos et al. (2011) previously proposed the structure of OP282 b/c in Figure
448 4 based on HRMS measurements and the fragmentation pattern observed, which
449 agrees with the results obtained in our work. For the formation of OP282 b/c (Figure 7)
450 two oxidation equivalents were considered to propose a possible formation pathway.
451 Here the initiation of the reaction could also start as the suggested pathway C for the
452 formation of NIT (Figure 6, reaction (7)-(10)), with the difference that the reaction at
453 the nitrogen would terminate after formation of the nitroso-group and the second ozone
454 attack would follow an oxygen transfer at the aromatic ring (pathway D) (SI, Figure S
455 9). The reason for suggesting the aromatic ring as one of the reaction sites for ozone
456 is due to the observed retention times for OP282 b/c (OP282b R_t : 6.7 min, OP282c R_t :
457 7.1 min) and their fragmentation patterns (SI, Figure S 11, Figure S 12). Furthermore,
458 these two isomers are clearly not related to NIT, due to their significantly shorter
459 retention times (NIT R_t : 17.2 min).

460 According to the mass spectrometric fragmentation pattern observed for OP284 (SI,
 461 Figure S 13), this compound is formed by the addition of two oxygen atoms to the
 462 aniline ring structure (Figure 7). Its proposed structure presents hydroxylation at the
 463 nitrogen and the aromatic ring, but as mentioned above, only one of the two oxygens
 464 is labeled. Based on this observation, we propose that the labeled oxygen comes from
 465 the direct addition of ozone to the aromatic ring of the aniline (pathway D), while the
 466 second oxygen originates from an electron transfer reaction that occurs at the nitrogen
 467 moiety (SI, Figure S 8, pathway E). As mentioned in the previous section, the
 468 production of this OP was limited and some uncertainty remains regarding the
 469 possibility of both oxygen atoms having their origin in direct oxygen transfers from the
 470 ozone molecule.

471 The suggested reactions are summarized as a proposed pathway for the
 472 transformation of SMX in Figure 7. Some of the intermediates expected after the first
 473 ozone attack (nitroso sulfamethoxazole and sulfamethoxazole hydroxylamine) were
 474 not detected in this study, but the SMX hydroxylamine was reported previously (Willach
 475 et al., 2017). Nonetheless, the formation pathway proposed in Figure 7 agrees with
 476 those previously established by Von Sonntag and Von Gunten (2012); Willach et al.
 477 (2017).



478
 479 Figure 7. Overview of the formation pathways involved in the formation of six of the
 480 OPs of SMX. Detailed individual pathways are illustrated in Figures 7, S8, S9 and S10.
 481 Orange circles highlight the presence of ¹⁸O.

482 For the formation of OP269, we can exclude a two-step reaction involving the
 483 hydroxylation of the aromatic ring by an oxygen transfer reaction, due to the lack of

484 ¹⁸O-labeling observed in the formed OP (see Figure 5). Furthermore, our results agree
485 with the formation pathway proposed by Willach et al. (2017) for OP269, who
486 hypothesized that the formation pathway is initiated by an ozone reaction in the
487 aromatic ring, resulting in an electron transfer reaction (SI, Figure S 10, pathway F).
488 The following reactions result in the cleavage of the anilinic nitrogen from the aromatic
489 ring and its replacement by a quinone group (Willach et al., 2017).

490 Only one form of OP226 could be detected in the different ozonation experiments,
491 unlike the two isomers reported by (Willach et al., 2017). Therefore, it can be concluded
492 that the OP226 detected is not being produced by the reaction of SMX with a hydroxyl
493 radical because of the presence of a radical scavenger. Furthermore, it can be stated
494 with some certainty that the formation pathway involves the transfer of one oxygen
495 atom from ozone.

496 Overall, the successful labeling of six of the seven detected SMX OPs confirmed the
497 applicability of the new method to track the formation of ozonation products from
498 compounds with aniline moieties. Furthermore, the ¹⁸O/¹⁶O ratio provided by the
499 labeling of NOV was paramount to understand the origin of the transferred oxygen
500 atoms and thereby supported the differentiation of previously proposed transformation
501 pathways from oxygen transfer or electron transfer reactions.

502 4. Conclusions

503 This study presented a novel labeling technique with the aim of generating transferable
504 knowledge of ozone reactions, as well as, elucidating formation pathways of OPs. The
505 major conclusions are:

- 506 • The formation of labeled venlafaxine N-oxide (+2 Da) confirmed the transfer of one
507 ¹⁸O atom to the tertiary amine of the model compound. The ratio of ¹⁸O/¹⁶O in the
508 formed venlafaxine N-oxide correlated with determined gas ratios in previous tracer
509 tests with N₂ and O₂ at the same operational settings. Therefore, venlafaxine N-
510 oxide can be used as an indicator of ¹⁸O purity in the system. The measured ¹⁸O/¹⁶O
511 ratios obtained from NOV formation can be used to confirm the origin of the
512 transferred oxygens in newly formed OPs.
- 513 • The results corroborate that the labeling technique can be used to study the reaction
514 mechanism of ozone, when a transfer of oxygen is involved. Consequently, we

515 present the use of $^{18}\text{O}_3$ as a suitable tool to investigate the reaction of ozone with
516 organic chemicals in a wide range of scenarios.

- 517 • Besides the observed suitability for the elucidation of formation mechanisms and
518 pathways, the integration of this new labeling method will enable the detection of
519 OPs from chemicals with multiple reactive sites and in complex water matrices. In a
520 parallel study this approach has already been applied to identify OBPs formed when
521 effluent organic matter from secondary effluent is ozonated.
- 522 • An additional potential application of this labeling method is the tracking of OPs and
523 their characteristic newly formed functional groups in biological post-treatment to
524 better understand their stability and persistence in the environment. The presence
525 of the labeled functional group can be used to assess the generation of recalcitrant
526 and potentially toxic OPs in complex water scenarios.

527 5. Declaration of Competing Interest

528 The authors declare no known competing financial interest or personal relationship that
529 could have influence on the work reported in this paper.

530 6. Acknowledgments

531 This study was funded by the Deutsche Forschungsgemeinschaft (DFG-German
532 Research Foundation) under the Project Numbers 428639365 (GZ: HU 2699/1-1 and
533 RE 1290/8-1). We would like to thank Danika Ahoor (TUM) for her contributions in
534 solving the gas humidity problems, Dr. Ignacio Sottorff (TUM) for his consistent support
535 and understanding, and Elaine Jennings (UFZ) for feedback and discussion.

536 7. References

- 537 Bader, H. 1982. Determination of Ozone In Water By The Indigo Method: A Submitted
538 Standard Method. *Ozone: Science & Engineering* 4(4), 169-176.
539 <https://doi.org/10.1080/01919518208550955>.
- 540 Betsholtz, A., Juárez, R., Svahn, O., Davidsson, Å., Cimbritz, M. and Falås, P. 2022.
541 Ozonation of ^{14}C -labeled micropollutants – mineralization of labeled moieties and
542 adsorption of transformation products to activated carbon. *Water Research* 221,
543 118738. <https://doi.org/10.1016/j.watres.2022.118738>.
- 544 Borowska, E., Bourgin, M., Hollender, J., Kienle, C., McArdell, C.S. and von Gunten, U. 2016.
545 Oxidation of cetirizine, fexofenadine and hydrochlorothiazide during ozonation: Kinetics
546 and formation of transformation products. *Water Research* 94, 350-362.
547 <https://doi.org/10.1016/j.watres.2016.02.020>.

- 548 Bourgin, M., Beck, B., Boehler, M., Borowska, E., Fleiner, J., Salhi, E., Teichler, R., von
549 Gunten, U., Siegrist, H. and McArdell, C.S. 2018. Evaluation of a full-scale wastewater
550 treatment plant upgraded with ozonation and biological post-treatments: Abatement of
551 micropollutants, formation of transformation products and oxidation by-products. *Water*
552 *Research* 129, 486-498. <https://doi.org/10.1016/j.watres.2017.10.036>.
- 553 Brunner, A.M., Vughs, D., Siegers, W., Bertelkamp, C., Hofman-Caris, R., Kolkman, A. and ter
554 Laak, T. 2019. Monitoring transformation product formation in the drinking water
555 treatments rapid sand filtration and ozonation. *Chemosphere* 214, 801-811.
556 <https://doi.org/10.1016/j.chemosphere.2018.09.140>.
- 557 Dodd, M.C. and Huang, C.-H. 2004. Transformation of the Antibacterial Agent
558 Sulfamethoxazole in Reactions with Chlorine: Kinetics, Mechanisms, and Pathways.
559 *Environmental Science & Technology* 38(21), 5607-5615.
560 <https://doi.org/10.1021/es035225z>.
- 561 Dodd, M.C., Rentsch, D., Singer, H.P., Kohler, H.-P.E. and von Gunten, U. 2010.
562 Transformation of β -Lactam Antibacterial Agents during Aqueous Ozonation: Reaction
563 Pathways and Quantitative Bioassay of Biologically-Active Oxidation Products.
564 *Environmental Science & Technology* 44(15), 5940-5948.
565 <https://doi.org/10.1021/es101061w>.
- 566 Eggen, R.I.L., Hollender, J., Joss, A., Schäfer, M. and Stamm, C. 2014. Reducing the
567 Discharge of Micropollutants in the Aquatic Environment: The Benefits of Upgrading
568 Wastewater Treatment Plants. *Environmental Science & Technology* 48(14), 7683-
569 7689. <https://doi.org/10.1021/es500907n>.
- 570 Gao, S., Zhao, Z., Xu, Y., Tian, J., Qi, H., Lin, W. and Cui, F. 2014. Oxidation of
571 sulfamethoxazole (SMX) by chlorine, ozone and permanganate - A comparative study.
572 *Journal of Hazardous Materials* 274, 258-269.
573 <https://doi.org/10.1016/j.jhazmat.2014.04.024>.
- 574 Gómez-Ramos, M.d.M., Mezcua, M., Agüera, A., Fernández-Alba, A.R., Gonzalo, S.,
575 Rodríguez, A. and Rosal, R. 2011. Chemical and toxicological evolution of the
576 antibiotic sulfamethoxazole under ozone treatment in water solution. *Journal of*
577 *Hazardous Materials* 192(1), 18-25. <https://doi.org/10.1016/j.jhazmat.2011.04.072>.
- 578 Gulde, R., Clerc, B., Rutsch, M., Helbing, J., Salhi, E., McArdell, C.S. and von Gunten, U.
579 2021. Oxidation of 51 micropollutants during drinking water ozonation: Formation of
580 transformation products and their fate during biological post-filtration. *Water Research*
581 207, 117812. <https://doi.org/10.1016/j.watres.2021.117812>.
- 582 Huber, M.M., Göbel, A., Joss, A., Hermann, N., Löffler, D., McArdell, C.S., Ried, A., Siegrist,
583 H., Ternes, T.A. and von Gunten, U. 2005. Oxidation of Pharmaceuticals during
584 Ozonation of Municipal Wastewater Effluents: A Pilot Study. *Environmental Science &*
585 *Technology* 39(11), 4290-4299. <https://doi.org/10.1021/es048396s>.
- 586 Huber, M.M., Ternes, T.A. and von Gunten, U. 2004. Removal of Estrogenic Activity and
587 Formation of Oxidation Products during Ozonation of 17α -Ethinylestradiol.
588 *Environmental Science & Technology* 38(19), 5177-5186.
589 <https://doi.org/10.1021/es035205x>.
- 590 Hübner, U., von Gunten, U. and Jekel, M. 2015. Evaluation of the persistence of
591 transformation products from ozonation of trace organic compounds—a critical review.
592 *Water Research* 68, 150-170. <https://doi.org/10.1016/j.watres.2014.09.051>.
- 593 Jennings, E., Sierra Olea, M., Michael Kaesler, J., Hübner, U., Reemtsma, T. and Lechtenfeld,
594 O.J. under review. Stable Isotope Labeling for Detection of Ozonation Byproducts in
595 Effluent Organic Matter with FT-ICR-MS. *Water Research*.
- 596 Kolkman, A., Martijn, B.J., Vughs, D., Baken, K.A. and van Wezel, A.P. 2015. Tracing
597 Nitrogenous Disinfection Byproducts after Medium Pressure UV Water Treatment by
598 Stable Isotope Labeling and High Resolution Mass Spectrometry. *Environmental*
599 *Science & Technology* 49(7), 4458-4465. <https://doi.org/10.1021/es506063h>.
- 600 Lee, Y. and Von Gunten, U. 2016. Advances in predicting organic contaminant abatement
601 during ozonation of municipal wastewater effluent: reaction kinetics, transformation
602 products, and changes of biological effects. *Environmental Science: Water Research*
603 *& Technology* 2(3), 421-442. <https://doi.org/10.1039/C6EW00025H>.

- 604 Lim, S., McArdell, C.S. and von Gunten, U. 2019. Reactions of aliphatic amines with ozone:
605 Kinetics and mechanisms. *Water Research* 157, 514-528.
606 <https://doi.org/10.1016/j.watres.2019.03.089>.
- 607 Lim, S., Shi, J.L., von Gunten, U. and McCurry, D.L. 2022. Ozonation of Organic Compounds
608 in Water and Wastewater: A Critical Review. *Water Research*, 118053.
609 <https://doi.org/10.1016/j.watres.2022.118053>.
- 610 Liu, Z., Craven, C.B., Huang, G., Jiang, P., Wu, D. and Li, X.-F. 2019. Stable Isotopic Labeling
611 and Nontarget Identification of Nanogram/Liter Amino Contaminants in Water.
612 *Analytical Chemistry* 91(20), 13213-13221.
613 <https://doi.org/10.1021/acs.analchem.9b03642>.
- 614 Loos, M., Gerber, C., Corona, F., Hollender, J. and Singer, H. 2015. Accelerated isotope fine
615 structure calculation using pruned transition trees. *Analytical Chemistry* 87(11), 5738-
616 5744. <https://doi.org/10.1021/acs.analchem.5b00941>.
- 617 Loos, R., Carvalho, R., António, D.C., Comero, S., Locoro, G., Tavazzi, S., Paracchini, B.,
618 Ghiani, M., Lettieri, T., Blaha, L., Jarosova, B., Voorspoels, S., Servaes, K., Haglund,
619 P., Fick, J., Lindberg, R.H., Schwesig, D. and Gawlik, B.M. 2013. EU-wide monitoring
620 survey on emerging polar organic contaminants in wastewater treatment plant
621 effluents. *Water Research* 47(17), 6475-6487.
622 <https://doi.org/10.1016/j.watres.2013.08.024>.
- 623 Mairinger, T. and Hann, S. (2020) *Metabolic Flux Analysis in Eukaryotic Cells: Methods and*
624 *Protocols*. Nagraath, D. (ed), pp. 1-16, Springer US, New York, NY.
625 https://doi.org/10.1007/978-1-0716-0159-4_1.
- 626 Margot, J., Kienle, C., Magnet, A., Weil, M., Rossi, L., de Alencastro, L.F., Abegglen, C.,
627 Thonney, D., Chèvre, N., Schärer, M. and Barry, D.A. 2013. Treatment of
628 micropollutants in municipal wastewater: Ozone or powdered activated carbon?
629 *Science of the Total Environment* 461-462, 480-498.
630 <https://doi.org/10.1016/j.scitotenv.2013.05.034>.
- 631 Mawhinney, D.B., Vanderford, B.J. and Snyder, S.A. 2012. Transformation of 1H-
632 Benzotriazole by Ozone in Aqueous Solution. *Environmental Science & Technology*
633 46(13), 7102-7111. <https://doi.org/10.1021/es300338e>.
- 634 Müller, J., Drewes, J.E. and Hübner, U. 2017. Sequential biofiltration–A novel approach for
635 enhanced biological removal of trace organic chemicals from wastewater treatment
636 plant effluent. *Water Research* 127, 127-138.
637 <https://doi.org/10.1016/j.watres.2017.10.009>.
- 638 Müller, J., Drewes, J.E. and Hübner, U. 2019. Investigating synergies in sequential
639 biofiltration-based hybrid systems for the enhanced removal of trace organic chemicals
640 from wastewater treatment plant effluents. *Environmental Science: Water Research &*
641 *Technology* 5(8), 1423-1435. <https://doi.org/10.1039/C9EW00181F>.
- 642 Real, F.J., Benitez, F.J., Acero, J.L., Sagasti, J.J.P. and Casas, F. 2009. Kinetics of the
643 Chemical Oxidation of the Pharmaceuticals Primidone, Ketoprofen, and Diatrizoate in
644 Ultrapure and Natural Waters. *Industrial & Engineering Chemistry Research* 48(7),
645 3380-3388. <https://doi.org/10.1021/ie801762p>.
- 646 Reemtsma, T., Weiss, S., Mueller, J., Petrovic, M., González, S., Barcelo, D., Ventura, F. and
647 Knepper, T.P. 2006. Polar Pollutants Entry into the Water Cycle by Municipal
648 Wastewater: A European Perspective. *Environmental Science & Technology* 40(17),
649 5451-5458. <https://doi.org/10.1021/es060908a>.
- 650 Spahr, S., Bolotin, J., Schleucher, J., Ehlers, I., von Gunten, U. and Hofstetter, T.B. 2015.
651 Compound-Specific Carbon, Nitrogen, and Hydrogen Isotope Analysis of N-
652 Nitrosodimethylamine in Aqueous Solutions. *Analytical Chemistry* 87(5), 2916-2924.
653 <https://doi.org/10.1021/ac5044169>.
- 654 Spahr, S., von Gunten, U. and Hofstetter, T.B. 2017. Carbon, Hydrogen, and Nitrogen Isotope
655 Fractionation Trends in N-Nitrosodimethylamine Reflect the Formation Pathway during
656 Chloramination of Tertiary Amines. *Environmental Science & Technology* 51(22),
657 13170-13179. <https://doi.org/10.1021/acs.est.7b03919>.

- 658 Tekle-Röttering, A., von Sonntag, C., Reisz, E., Eyser, C.v., Lutze, H.V., Türk, J., Naumov, S.,
659 Schmidt, W. and Schmidt, T.C. 2016. Ozonation of anilines: Kinetics, stoichiometry,
660 product identification and elucidation of pathways. *Water Research* 98, 147-159.
661 <https://doi.org/10.1016/j.watres.2016.04.001>.
- 662 Tentscher, P.R., Lee, M. and von Gunten, U. 2019. Micropollutant Oxidation Studied by
663 Quantum Chemical Computations: Methodology and Applications to Thermodynamics,
664 Kinetics, and Reaction Mechanisms. *Accounts of Chemical Research* 52(3), 605-614.
665 <https://doi.org/10.1021/acs.accounts.8b00610>.
- 666 Ternes, T.A., Stüber, J., Herrmann, N., McDowell, D., Ried, A., Kampmann, M. and Teiser, B.
667 2003. Ozonation: a tool for removal of pharmaceuticals, contrast media and musk
668 fragrances from wastewater? *Water Research* 37(8), 1976-1982.
669 [https://doi.org/10.1016/S0043-1354\(02\)00570-5](https://doi.org/10.1016/S0043-1354(02)00570-5).
- 670 Valkenburg, D., Mertens, I., Lemière, F., Witters, E. and Burzykowski, T. 2012. The isotopic
671 distribution conundrum. *Mass Spectrometry Reviews* 31(1), 96-109.
672 <https://doi.org/10.1002/mas.20339>.
- 673 von Gunten, U. 2003. Ozonation of drinking water: Part I. Oxidation kinetics and product
674 formation. *Water Research* 37(7), 1443-1467. [https://doi.org/10.1016/S0043-
675 1354\(02\)00457-8](https://doi.org/10.1016/S0043-1354(02)00457-8).
- 676 von Gunten, U. 2018. Oxidation Processes in Water Treatment: Are We on Track?
677 *Environmental Science & Technology* 52(9), 5062-5075.
678 <https://doi.org/10.1021/acs.est.8b00586>.
- 679 Von Sonntag, C. and Von Gunten, U. (2012) *Chemistry of ozone in water and wastewater*
680 *treatment*, IWA publishing. <https://doi.org/10.2166/9781780400839>.
- 681 Wert, E.C., Rosario-Ortiz, F.L., Drury, D.D. and Snyder, S.A. 2007. Formation of oxidation
682 byproducts from ozonation of wastewater. *Water Research* 41(7), 1481-1490.
683 <https://doi.org/10.1016/j.watres.2007.01.020>.
- 684 Willach, S., Lutze, H.V., Eckey, K., Löppenberg, K., Lüling, M., Terhalle, J., Wolbert, J.-B.,
685 Jochmann, M.A., Karst, U. and Schmidt, T.C. 2017. Degradation of sulfamethoxazole
686 using ozone and chlorine dioxide - Compound-specific stable isotope analysis,
687 transformation product analysis and mechanistic aspects. *Water Research* 122, 280-
688 289. <https://doi.org/10.1016/j.watres.2017.06.001>.
- 689 Yu, H., Ge, P., Chen, J., Xie, H. and Luo, Y. 2017. The degradation mechanism of
690 sulfamethoxazole under ozonation: a DFT study. *Environmental Science: Processes &*
691 *Impacts* 19(3), 379-387. <https://doi.org/10.1039/C6EM00698A>.
- 692 Zucker, I., Mamane, H., Riani, A., Gozlan, I. and Avisar, D. 2018. Formation and degradation
693 of N-oxide venlafaxine during ozonation and biological post-treatment. *Science of the*
694 *Total Environment* 619, 578-586. <https://doi.org/10.1016/j.scitotenv.2017.11.133>.
- 695

Supplementary Information

Isotopically labeled ozone in functional group ozonation: a new approach for elucidating ozonation products formation

Millaray Sierra Olea^a, Simon Kölle^a, Emil Bein^a, Thorsten Reemtsma^b, Oliver J. Lechtenfeld^b, and Uwe Hübner^{a*}

^a Chair of Urban Water Systems Engineering, Technical University of Munich, Am Coulombwall 3, D-85748 Garching, Germany

^b Department of Analytical Chemistry, Helmholtz Centre for Environmental Research – UFZ, Permoserstrasse 15, 04318 Leipzig, Germany

* Corresponding author: Chair of Urban Water Systems Engineering, Technical University of Munich, Am Coulombwall 3, D-85748 Garching, Germany

E-mail: u.huebner@tum.de (U. Hübner)

Table of Contents

Supplementary Information.....	3
Table S 1: List of used chemicals.....	3
Figure S 1: Design of an ozonation system modified for oxidation with ¹⁸ O ₂	4
Table S 2: List of the equipment, materials and chemicals used for the ozonation setup.	4
Table S 3: Batch experiment sample composition.	5
Table S 4: Targeted molar ratios for the ozonation of compounds.....	5
Table S 5: List of compounds measured with the MRM method.	5
Table S 6: Gradient Method.	6
Table S 7: Mass ranges used in MS ¹ and MS ² experiments.	6
Table S 8: Isotopologue peaks ranges of MS ¹ scans, focusing on their centroid mass (Da), peak start (Da) and peak end (Da).	6
Table S 9: Ranges used for the area integration of the detected SMX OPs. ...	9
Text S 1: Expected isotopic pattern of SMX + 2O using enviPat platform.	10
Figure S 2: Impact of gas pressure of the ozone generator on the expected purity of ¹⁸ O in the system.....	10
Figure S 3: Impact in the simulated gas purity depending on the gas being exchanged.	11

35	Text S 2: Correlation of the pressure with the oxygen measured by the in-line	
36	<i>PreSens</i> oxygen sensors (A. Schmid, personal communication May 25 th , 2022).	
37	11
38	Figure S 4: The reaction of VLX with O ₃ results in the transfer of one oxygen	
39	atom to the nitrogen in the tertiary amine moiety. From this reaction it has been	
40	reported a formation of >70% of NOV (Zucker et al., 2018).....	12
41	Text S 3: Isotope pattern determination for NOV using enviPat platform.	12
42	Figure S 5: 4-nitrosulfamethoxazole calibration curve (ng L ⁻¹).	13
43	Figure S 6: Yield of 4-nitrosulfamethoxazole (NIT). Three independent	
44	ozonation experiments were performed using different ¹⁸ O/ ¹⁶ O ratios for the	
45	production of ozone. The targeted SMX : O ₃ dose (see SI, Table A - 4) was the	
46	same in all experiments. Error bars indicate the standard deviation.	13
47	Figure S 7: Removal of SMX and formation of the seven OPs obtained from the	
48	ozonation experiments. These OPs are: (A) OP282a also identified as 4-nitro	
49	sulfamethoxazole (NIT), (B) OP282b, (C) OP282c, (D) OP284, (E) OP268, (F)	
50	OP269, and (G) OP226. The number is their m/z when produced by ¹⁶ O ₃	14
51	Figure S 8: Proposed reaction mechanism for the formation of the two isomers	
52	of OP268 in the reaction with ozone (pathway D and E). The detected OP268	
53	could be formed by an oxygen addition at the aromatic ring (Orange circle	
54	highlights the presence of oxygen-18). Meanwhile the undetected OP268, can	
55	be explained by the reaction with ozone and the subsequent formation of	
56	sulfamethoxazole hydroxylamine and 4 – nitroso sulfamethoxazole (Extracted	
57	Willach et al. (2017)).	15
58	Figure S 9: Proposed reaction mechanism for the formation of OP282 b/c and	
59	OP284 in the reaction with ozone. Orange circle highlights the presence of	
60	oxygen-18.	16
61	Figure S 10: Proposed reaction mechanism for the formation of OP269 in the	
62	reaction with ozone (Extracted from Willach et al. (2017)).	16
63	Figure S 11: Fragmentation pattern of OP282b, Rt: 6.7 min. A) ozone produced	
64	with technical oxygen (¹⁶ O ₂), B) ozone produced with 55% ¹⁸ O ₂ , C) ozone	
65	produced with 74% ¹⁸ O ₂	17
66	Figure S 12: Fragmentation pattern of OP282c, Rt: 6.7 min. A) ozone produced	
67	with technical oxygen (¹⁶ O ₂), B) ozone produced with 55% ¹⁸ O ₂ , C) ozone	
68	produced with 74% ¹⁸ O ₂	18
69	Figure S 13: Fragmentation pattern of OP284, Rt: 6.2 min. A) ozone produced	
70	with technical oxygen (¹⁶ O ₂), B) ozone produced with 55% ¹⁸ O ₂ , C) ozone	
71	produced with 74% ¹⁸ O ₂	19

73 **Supplementary Information**

74

75 Table S 1: List of used chemicals.

Chemicals	Supplier	CAS.No
Indigo Carmine, 80% purity	<i>Carl Roth GmbH, EG-No: 212-728-8</i>	
Labeled Oxygen (¹⁸ O ₂)	<i>97% purity, 1 bar, Linde Gas</i>	
Molecular Sieve / Zeolite	<i>0.3 nm, ~2 mm beads, Supelco, 1.05704.1000</i>	1318-02-1
Nitrogen (N ₂)	<i>≥ 99,8 %, “Nitrogen 2.8”, 300 bar, Air Liquide</i>	
Oxygen (¹⁶ O ₂)	<i>≥ 99,95 % “Oxygen 3.5”, 300 bar, Air Liquide</i>	
Phosphoric Acid	<i>85 %, Emsure, 1.00573.1000</i>	
Primidone	Fluka Analytics	125-33-7
Sulfamethoxazole	Fluka Analytics	723-46-6
4-Nitro Sulfamethoxazole	Toronto Research Chemicals	29699-89-6
tert-Butanol, ≥99.0 %	Carl Roth GmbH	75-65-0
Venlafaxine (VLX Hydrochlorid)	Sigma-Aldrich	99300-78-4
Venlafaxine N-Oxide	Toronto Research Chemicals	1094598-37-4

76

77

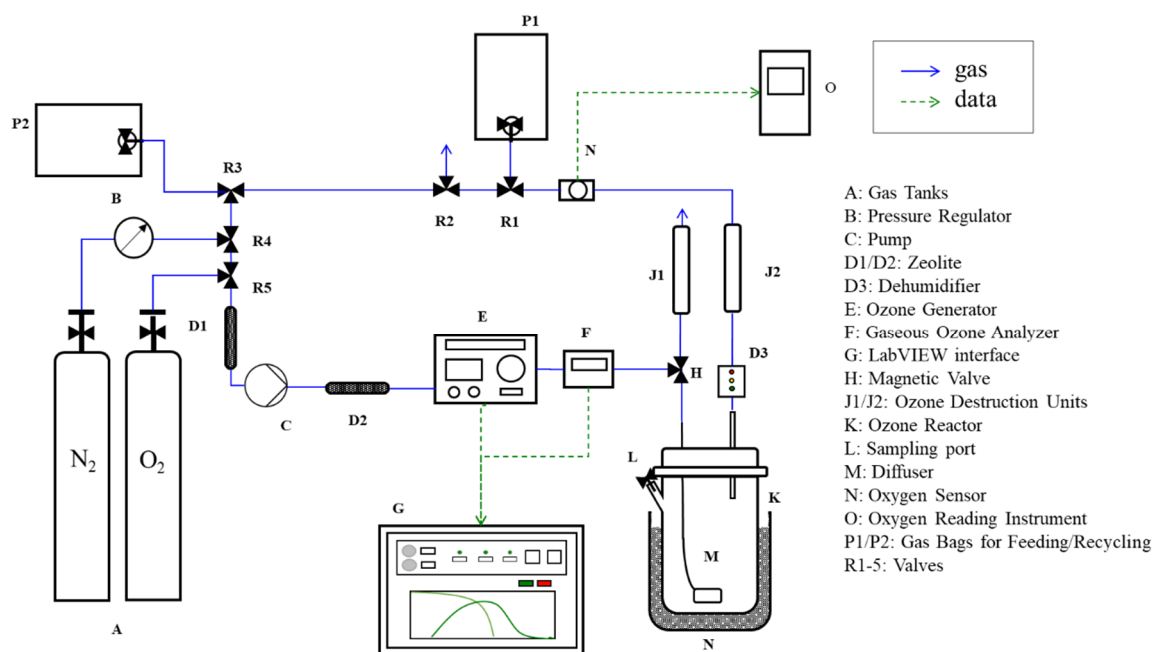


Figure S 1: Design of an ozonation system modified for oxidation with $^{18}\text{O}_2$.

Table S 2: List of the equipment, materials and chemicals used for the ozonation setup.

Gas bags (Q)	Bag, Multi-Layer, 3 Liter, Polypropylene Combo Valve with Replaceable Septum, 1 Eyelet, Catalog #: 22951. <i>Restek</i>
Hoses	Material: PTFE, 6/4x1. <i>Serto AG</i>
Magnetic Valve (H)	Plunger Valve 3/2-way direct acting, for liquid and gaseous media. Type 0355. <i>Bürkert – Fluid Control Systems</i>
Oxygen Reading Instrument (P)	Fibox 4 Fiber Optic Oxygen Transmitter. <i>PreSens Precision Sensing</i>
Oxygen Sensor (O)	Single-Use Flow-Through Cell O ₂ FTC-SU-PSt3. <i>Presens Precision Sensing</i>
Ozone Analyzer (F)	Ozone Analyzer BMT 964, in-gas (range: 300 g/Nm ³) off-gas (range: 50 g/Nm ³). <i>BMT Messtechnik GmbH</i>
Ozone Destruction Units (J)	CAT-RS. <i>BMT Messtechnik GmbH</i>
Ozone Generator (E)	BMT 803 BT (Bench Top), air cooled. <i>BMT Messtechnik GmbH</i>
Ozone Reactor (K)	Duran Glass Bottle (500 mL) with integrated outlet for the sampling port (L)
Pump (C)	MP-F05, Performance: 320 NI/H, <i>M&C TechGroup Germany GmbH</i>
Sampling syringes and needles	Long-life Instrument Syringe, 1 mL, 2.5 mL and 100 μL . <i>SGE</i>
Valve R1-3	3-way T ball valve with locking handle. <i>Osmobil</i>
Valve R4	ball valve, QH-QS-6-1/8 with plug connection. <i>Festo</i>

81

82 Table S 3: Batch experiment sample composition.

Sample	Compound Concentrations [$\mu\text{mol L}^{-1}$]				
	VLX	SMX	PRI	t-BuOH	Buffer
VLX #	20	0	3	10000	50000
SMX #	10	50	3	150000	50000

83

84 Table S 4: Targeted molar ratios for the ozonation of compounds.

VLX		VLX/SMX	
Ozone Conc. ($\mu\text{mol L}^{-1}$)	Molar Ratio VLX : O ₃	Ozone Conc. ($\mu\text{mol L}^{-1}$)	Molar Ratio VLX/SMX : O ₃
0	1:0	0	1:0
10	1:0.5	50	1:1
20	1:1	100	1:2
30	1:1.5	150	1:3
40	1:2	200	1:4
60	1:2.5	250	1:5
80	1:3	300	1:6
100	1:5		

85

86 Table S 5: List of compounds measured with the MRM method.

Expected RT	Compound Name	IS Name	Q1 Mass	Q3 Mass
MRM positive mode				
4.03	Primidone	Primidone-d5	219.10	162.10
4.03	Primidone	Primidone-d5	219.10	119.00
4.65	Venlafaxine	Venlafaxine-d6	278.20	215.20
4.65	Venlafaxine	Venlafaxine-d6	278.20	58.00
4.91	Venlafaxine N-oxid	Venlafaxine-d6	294.10	178.00
4.91	Venlafaxine N-oxid	Venlafaxine-d6	294.10	120.90
4.91	Venlafaxine N-oxid	Venlafaxine-d6	294.10	163.00
4.91	Venlafaxine N-oxid ¹⁸ O	Venlafaxine-d6	296.10	178.00
4.91	Venlafaxine N-oxid ¹⁸ O	Venlafaxine-d6	296.10	120.90
4.91	Venlafaxine N-oxid ¹⁸ O	Venlafaxine-d6	296.10	165.00
4.75	Sulfamethoxazole	Sulfamethoxazole-d4	254.00	156.00
4.75	Sulfamethoxazole	Sulfamethoxazole-d4	254.00	108.00
MRM negative mode				
5.71	4-Nitro Sulfamethoxazole	Cardersartan_d4	282.00	185.90

5.71	4-Nitro Sulfamethoxazole	Cardersartan_d4	282.00	137.90
5.71	4-Nitro Sulfamethoxazole	Cardersartan_d4	284.00	187.90
5.71	4-Nitro Sulfamethoxazole	Cardersartan_d4	284.00	139.90
5.71	4-Nitro Sulfamethoxazole	Cardersartan_d4	286.00	189.90
5.71	4-Nitro Sulfamethoxazole	Cardersartan_d4	286.00	141.90

87

88 Table S 6: Gradient Method.

Time [m]	Composition	
	Mobile Phase-A [%] (Water + 0.1%FA)	Mobile Phase-B [%] (ACN + 0.1%FA)
0.0	100	0
3.5	85	15
7.0	81	19
10.0	75	25
13.0	65	35
15.0	65	35
16.0	0	100
19.0	0	100
19.5	100	0
22.0	100	0

89

90 Table S 7: Mass ranges used in MS¹ and MS² experiments.

Scan Type	Mass range [Da]	
	Start	Stop
Enhanced MS Scan (EMS)	224.000	232.000
	280.000	290.000
	266.000	272.000
Enhanced Product Ion Scan (EPI)	90.000	300.000

91

92 Table S 8: Isotopologue peaks ranges of MS¹ scans, focusing on their centroid mass
93 (Da), peak start (Da) and peak end (Da).

	<i>m/z</i>	Centroid mass (Da)	Peak start (da)	Peak End (Da)
282a Rt: 17.2 min				
282				
Ave	282.10	282.10	281.88	282.32
std	0.1829758	0.1810161	0.2567650	0.1803999
min	282.000	281.880	281.640	282.000
max	282.72	282.72	282.88	282.84
284				
Ave	284.164557	284.1540456	284.0020253	284.3043038
std	0.178544023	0.175486081	0.21563201	0.182518829
min	284.04	283.92	283.68	284.04
max	284.88	284.88	284.88	285.24

286				
Ave	286.148	286.1375133	286.0093333	286.3
std	0.160049992	0.160239961	0.270443258	0.198595065
min	286.08	286.02	285.72	286.2
max	286.92	286.92	286.96	287.28
282b Rt: 6.7 min				
282				
Ave	282.1034483	282.1076506	281.9351724	282.2524138
std	0.216942323	0.232476324	0.250001665	0.211426276
min	282	281.88	281.76	282
max	282.96	283.2	282.96	283.2
284				
Ave	284.13	284.1218547	283.99875	284.240625
std	0.076485293	0.076262734	0.085430893	0.084997702
min	284.04	283.92	283.8	284.04
max	284.4	284.4	284.28	284.4
286				
Ave	286.1298113	286.1194094	285.9758491	286.2362264
std	0.067697735	0.056370554	0.073854369	0.082695769
min	286.08	286.05	285.84	286.08
max	286.32	286.32	286.2	286.32
282c Rt: 7.1 min				
282				
Ave	282.09	282.09	281.96	282.22
std	0.179452	0.178004	0.210577	0.177419
min	282.000	281.960	281.640	282.120
max	282.960	282.960	282.960	283.080
284				
Ave	284.1381818	284.1272515	284.0254545	284.2254545
std	0.062350648	0.072211432	0.082281516	0.089072354
min	284.04	283.92	283.8	284.04
max	284.28	284.28	284.16	284.4
286				
Ave	286.1217391	286.1004348	285.9634783	286.226087
std	0.075966364	0.086701801	0.18231861	0.086363193
min	286.08	285.96	285.2	286.08
max	286.32	286.32	286.2	286.44
284 Rt: 6.5 min				
284				
Ave	284.1307317	284.130439	283.9912195	284.2507317

non-peer reviewed EarthArXiv preprint – submitted and under review in “Water Research”

std	0.07853507	0.076173678	0.092451573	0.069013616
min	284.040	284.040	283.800	284.160
max	284.400	284.400	284.280	284.400
286				
Ave	286.1509091	286.1314545	286.0309091	286.2381818
std	0.078097206	0.096214121	0.093366779	0.075776967
min	286.08	285.96	285.84	286.08
max	286.32	286.32	286.2	286.32
268 Rt: 9.8 min				
268				
Ave	268.1132039	268.0991117	267.9401942	268.2518447
std	0.138200738	0.13666597	0.164346193	0.146861982
min	267.96	267.84	267.72	267.96
max	268.92	268.92	268.92	269.04
270				
Ave	270.1730435	270.169642	270.0052174	270.326087
std	0.18331334	0.183825488	0.22233679	0.183865242
min	270	270	269.76	270.12
max	270.96	270.96	270.96	271.32
269 Rt: 10.1				
269				
Ave	269.1361932	269.1201903	268.9670455	269.2504545
std	0.129113002	0.142658273	0.141855873	0.22567026
min	269.04	268.04	268.8	268.28
max	269.92	269.64	269.64	269.76
270				
Ave	270.1169231	270.1076	270.0292308	270.2092308
std	0.108655037	0.100389336	0.092525384	0.091016612
min	270	270	269.88	270.12
max	270.48	270.48	270.36	270.48
271				
Ave	271.1142857	271.0919048	271	271.16
std	0.091785019	0.065291949	0.06761234	0.06761234
min	270.96	270.96	270.84	271.08
max	271.44	271.2	271.08	271.32
226 Rt: 9.8 min				
226				
Ave	226.1014286	226.0822321	225.8657143	226.2428571
std	0.091014688	0.087382856	0.117212523	0.091918331
min	226.08	226.0036	225.72	226.08

max	226.56	226.5	226.32	226.56
228				
Ave	228.1285714	228.0857143	228	228.1457143
std	0.084418781	0.095447389	0.07855844	0.080862695
min	228	227.88	227.88	228
max	228.24	228.24	228.12	228.36

94

95 Table S 9: Ranges used for the area integration of the detected SMX OPs.

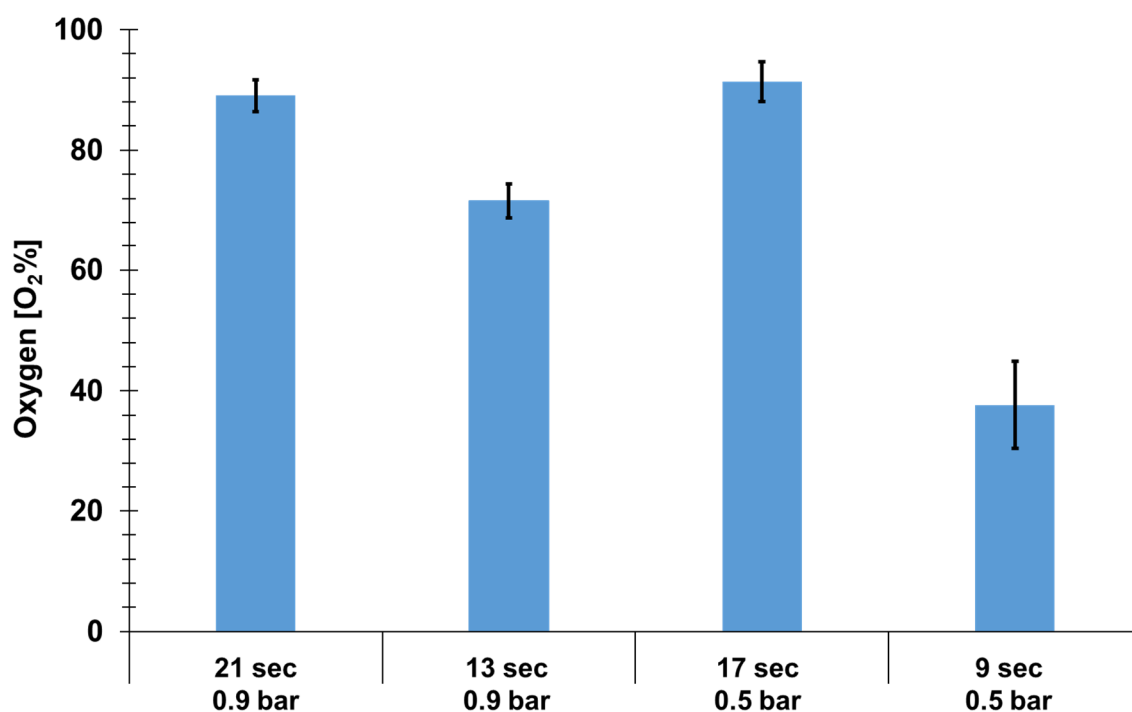
Name	Expected RT (min)	Mass Range [Da]	
		Start	Stop
TP284_1	6.5	283.8	284.4
TP284_2		285.8	286.4
TP282b_1	6.7	281.7	283.2
TP282b_2		283.8	284.4
TP282b_3		285.8	286.4
TP282c_1	7.1	281.6	283.1
TP282c_2		283.8	284.4
TP282c_3		285.2	286.5
TP226_1	9.8	225.7	226.6
TP226_2		227.8	228.4
TP268_1	9.8	267.7	269.1
TP268_2		296.7	271.4
TP269_1	10.1	268.8	269.8
TP269_2		269.9	270.5
TP269_3		270.9	271.4
TP282a_1	17.2	281.6	282.9
TP282a_2		283.6	285.3
TP282a_3		285.7	287.3

96

97

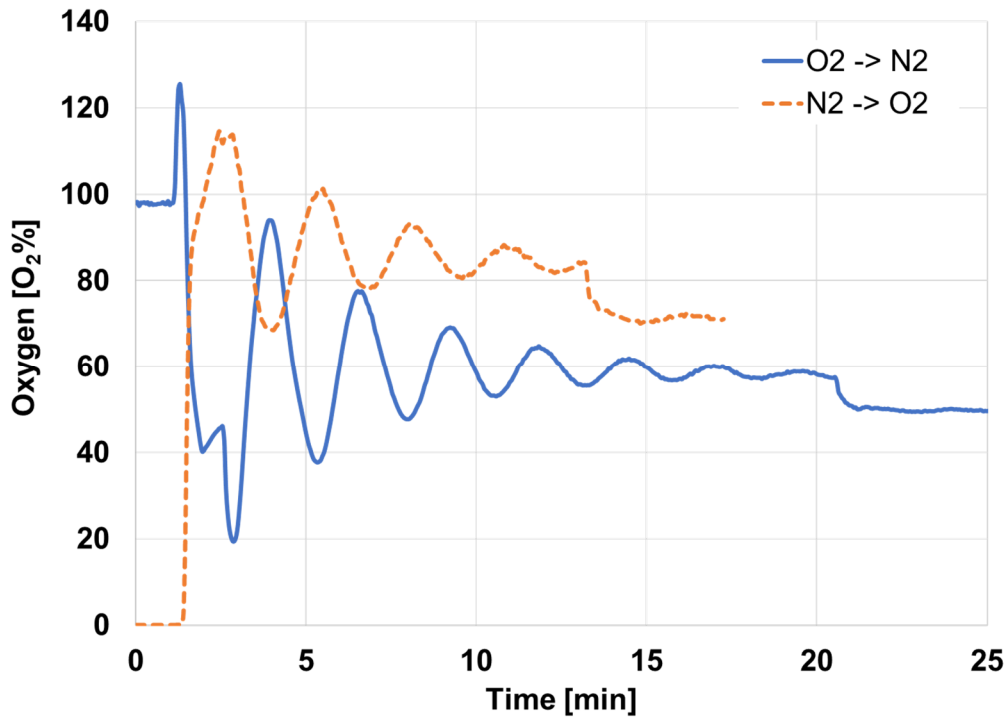
98 Text S 1: Expected isotopic pattern of SMX + 2O using enviPat platform.

99 The chemical formula of SMX + 2O isotopologues with relative abundances above the
100 threshold 0.01 were considered and their exact mass was calculated by replacing the
101 natural abundance of ^{16}O (99.757 %), and ^{18}O (0.205 %) (Coursey et al., 2015) and
102 using the calculated ratio of $^{16}\text{O}/^{18}\text{O}$ as indicated by the mass shift in NOV. The isotope
103 peaks that are relevant for SMX + 2O mass shift are: m/z 282 ($^{16}\text{O}_2$), m/z 284 ($^{16}\text{O}_1 -$
104 $^{18}\text{O}_1$) and m/z 286 ($^{18}\text{O}_2$) because of the expected shift in abundance occurs when the
105 direct reaction of ozone with the molecule is successful. According to the results of this
106 exercise, m/z 282 [M-H] $^-$ had a 100% of the relative abundance explained by the
107 chemical formula $^{12}\text{C}_{10}^{1}\text{H}_8^{14}\text{N}_3^{16}\text{O}_5^{32}\text{S}$. Meanwhile, m/z 284 [M-H] $^-$ is a sum of six
108 isotopologues with the isotope replacements of: ^{34}S (4.474 %), $^{13}\text{C} - ^{15}\text{N}$ (0.118 %),
109 $^{13}\text{C} - ^{33}\text{S}$ (0.085 %), ^{18}O (1.027 %), $^{13}\text{C}_2$ (0.526 %) and $^{13}\text{C} - ^{17}\text{O}$ (0.020 %). Finally,
110 m/z 286 [M-H] $^-$ is a sum of three isotopologues with the isotope replacements of:
111 ^{36}S (0.010 %), $^{18}\text{O} - ^{34}\text{S}$ (0.045 %) and $^{13}\text{C}_2 - ^{34}\text{S}$ (0.023 %). From these results we can
112 conclude that only ± 1.027 % of the 6.25 % relative abundance of m/z 284 can be
113 justified by the existence of one ^{18}O , meanwhile, ± 0.045 % of the relative abundance
114 of 0.080 % of m/z 286 can be expected to correspond to the presence of $^{18}\text{O} - ^{34}\text{S}$ in
115 the molecule.



116

117 Figure S 2: Impact of gas pressure of the ozone generator on the expected purity of
118 ^{18}O in the system.



119

120 Figure S 3: Impact in the simulated gas purity depending on the gas being exchanged.

121

122 Text S 2: Correlation of the pressure with the oxygen measured by the in-line *PreSens*
 123 oxygen sensors (A. Schmid, personal communication May 25th, 2022).

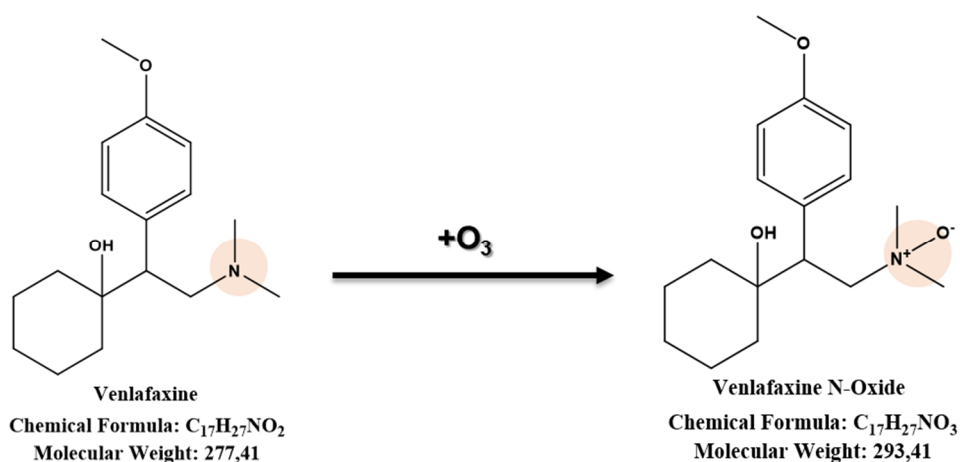
124
$$\% O_2(cor.) = \% O_2(meas.) \cdot \frac{p_{atm}}{p_{act}}$$

125

p_{atm}	Atmospheric pressure during calibration
p_{act}	Atmospheric pressure during measurement
$\% O_2(cor.)$	$\% O_2(cor.)$ corrected
$\% O_2(meas.)$	$\% O_2(meas.)$ measured

126

127



128

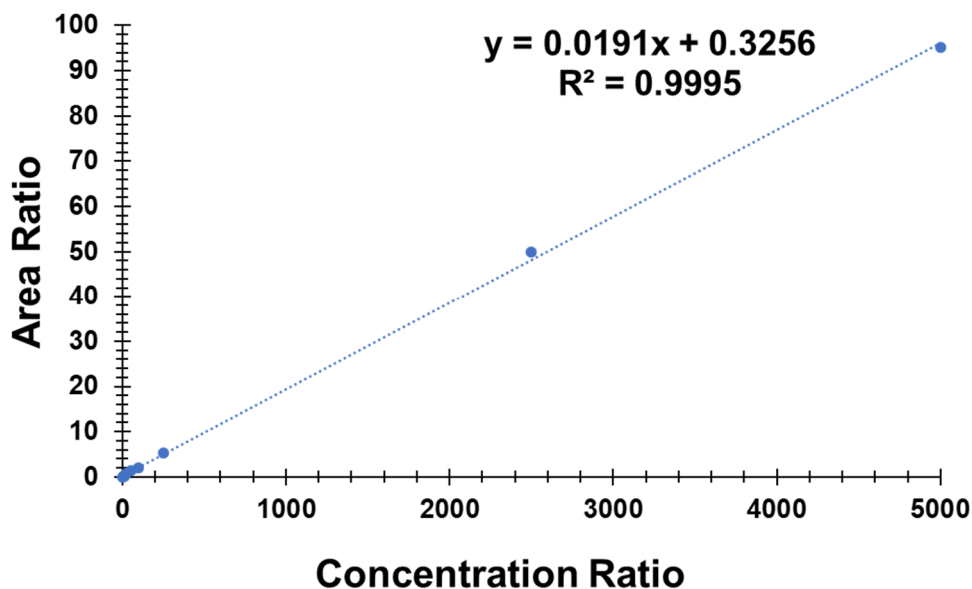
129 Figure S 4: The reaction of VLX with O_3 results in the transfer of one oxygen atom to
130 the nitrogen in the tertiary amine moiety. From this reaction it has been reported a
131 formation of >70% of NOV (Zucker et al., 2018).

132 Text S 3: Isotope pattern determination for NOV using enviPat platform.

133 According to the results of this exercise, m/z 294 had a 100 % of the relative
134 abundance explained by the chemical formula $^{12}C_{17}^{1}H_{28}^{14}N_1^{16}O_3$. Meanwhile, m/z 296
135 is a sum of five isotopologues with the isotope replacements of: $^{13}C - ^{15}N$ (0.067 %),
136 ^{18}O (0.616 %), $^{13}C_2$ (1.591 %), $^{13}C - ^{17}O$ (0.021 %) and $^{13}C - ^2H$ (0.059 %). Therefore,
137 only ± 0.616 % of the 3 % measured value can be justified by the existence of ^{18}O in
138 the molecule, and any change in the isotopic pattern of the molecule would be
139 explained by the reaction of VLX with $^{18}O_3$ and the attachment of one 18-oxygen atom
140 to the nitrogen group of the compound.

141

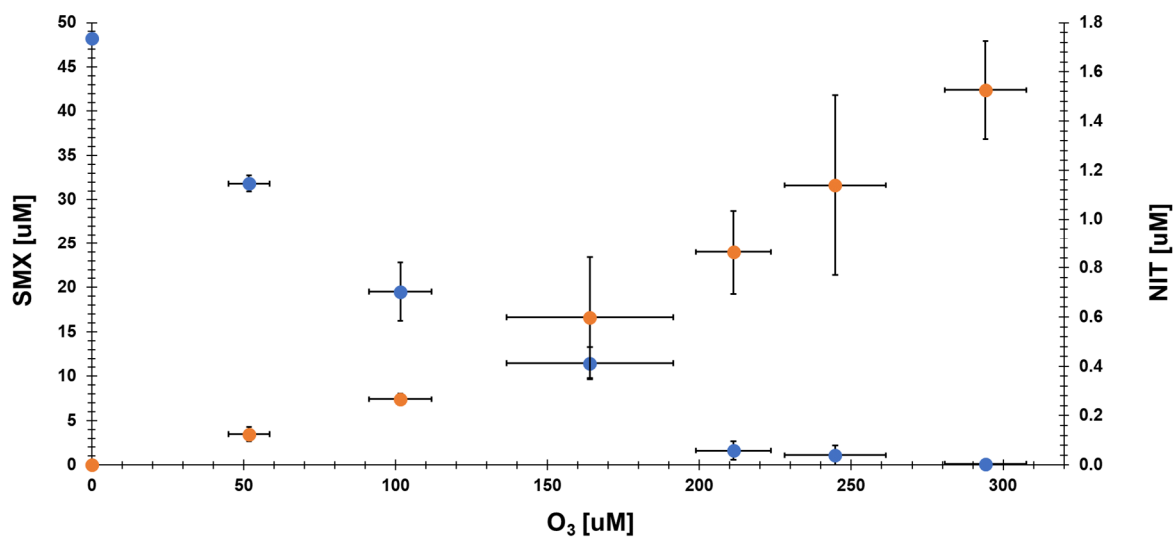
142



143

144 Figure S 5: 4-nitrosulfamethoxazole calibration curve (ng L⁻¹).

145

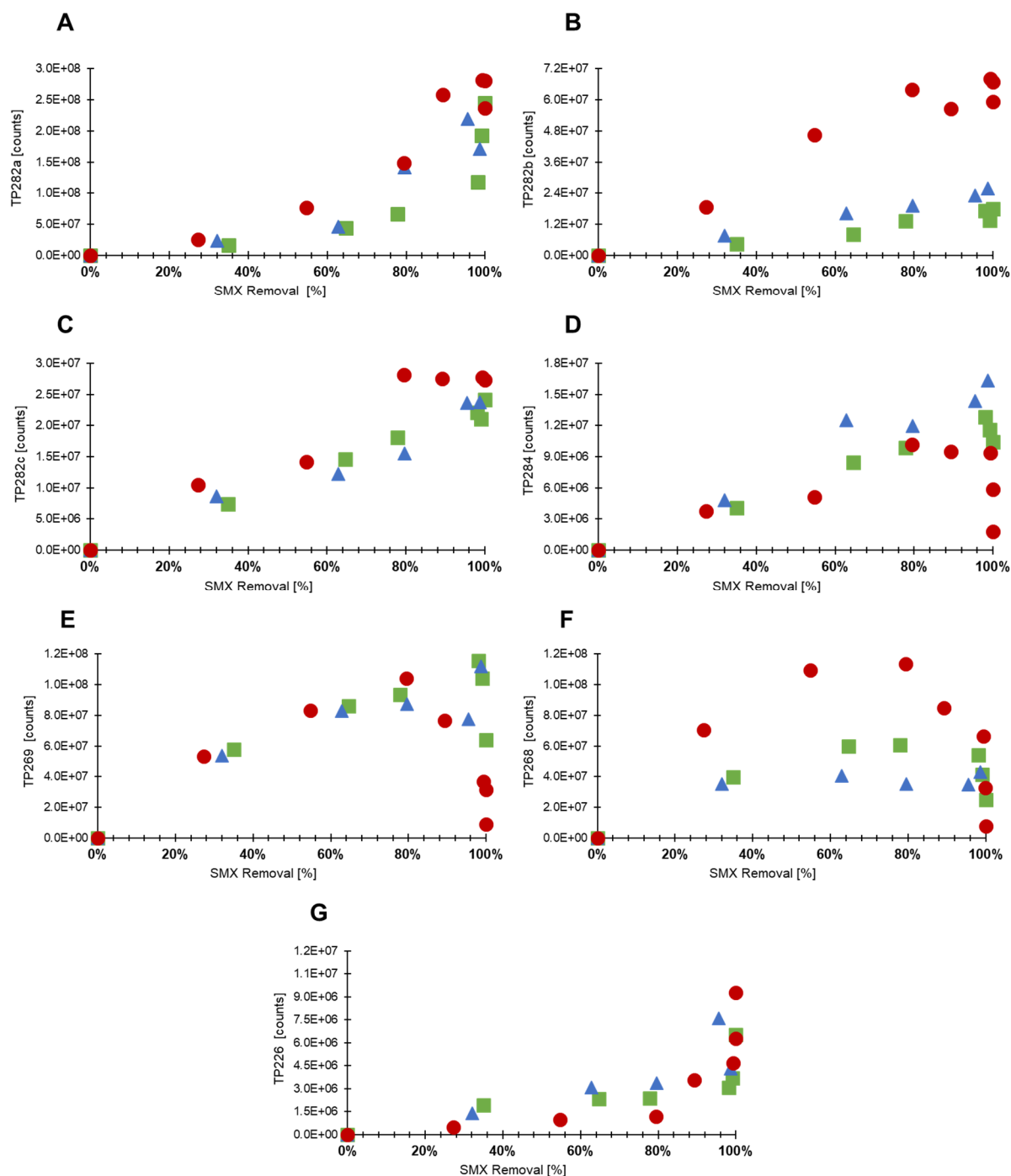


146

147 Figure S 6: Yield of 4-nitrosulfamethoxazole (NIT). Three independent ozonation
148 experiments were performed using different ¹⁸O/¹⁶O ratios for the production of ozone.
149 The targeted SMX : O₃ dose (see SI, **Error! Reference source not found.**) was the
150 same in all experiments. Error bars indicate the standard deviation.

151

152



153

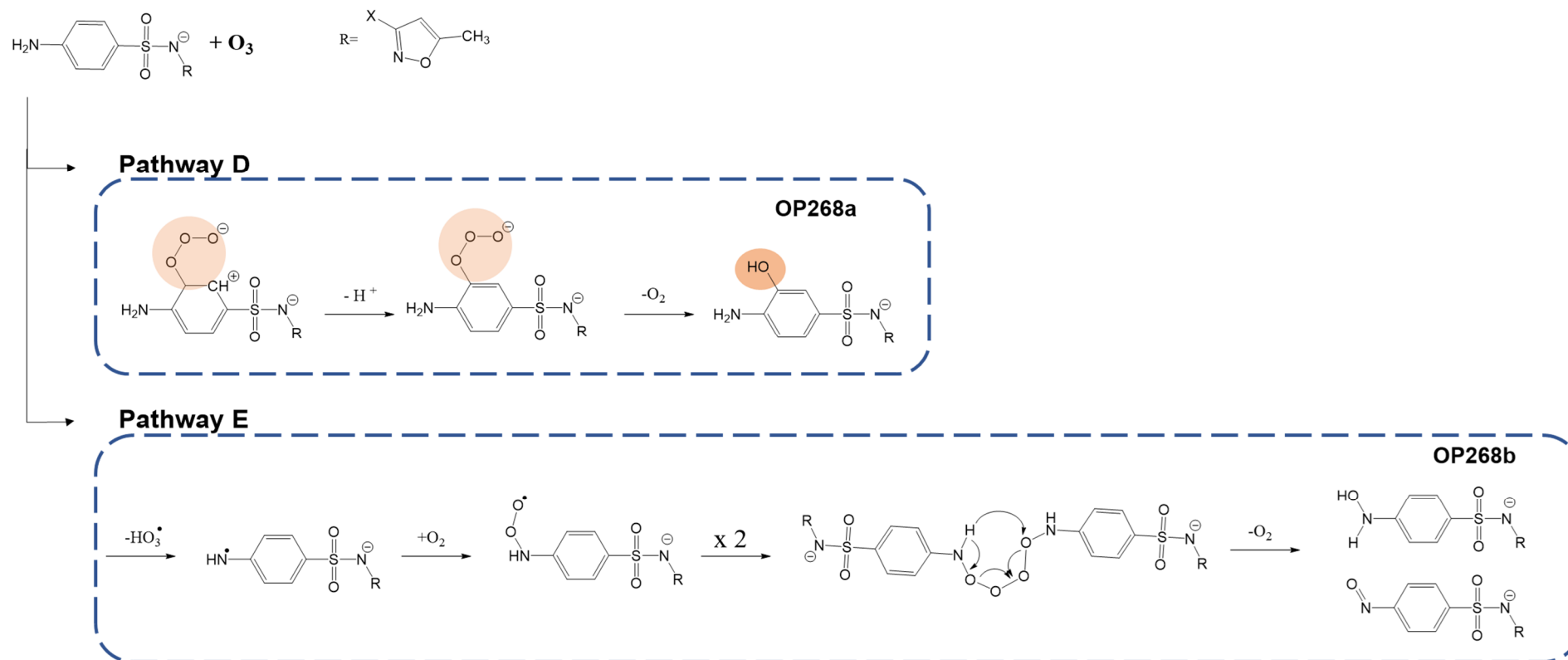
154

● $^{16}\text{O}_2$ ▲ $\sim 55\% \text{ }^{18}\text{O}_2$ ■ $\sim 74\% \text{ }^{18}\text{O}_2$

155

156 Figure S 7: Removal of SMX and formation of the seven OPs obtained from the
 157 ozonation experiments. These OPs are: (A) OP282a also identified as 4-nitro
 158 sulfamethoxazole (NIT), (B) OP282b, (C) OP282c, (D) OP284, (E) OP268, (F) OP269,
 159 and (G) OP226. The number is their m/z when produced by $^{16}\text{O}_3$.

160



161

162 Figure S 8: Proposed reaction mechanism for the formation of the two isomers of OP268 in the reaction with ozone (pathway D and E).
 163 The detected OP268a could be formed by an oxygen addition at the aromatic ring (Orange circle highlights the presence of oxygen-18).
 164 Meanwhile the undetected OP268b, can be explained by the reaction with ozone and the subsequent formation of sulfamethoxazole
 165 hydroxylamine and 4 – nitroso sulfamethoxazole (Extracted Willach et al. (2017)).

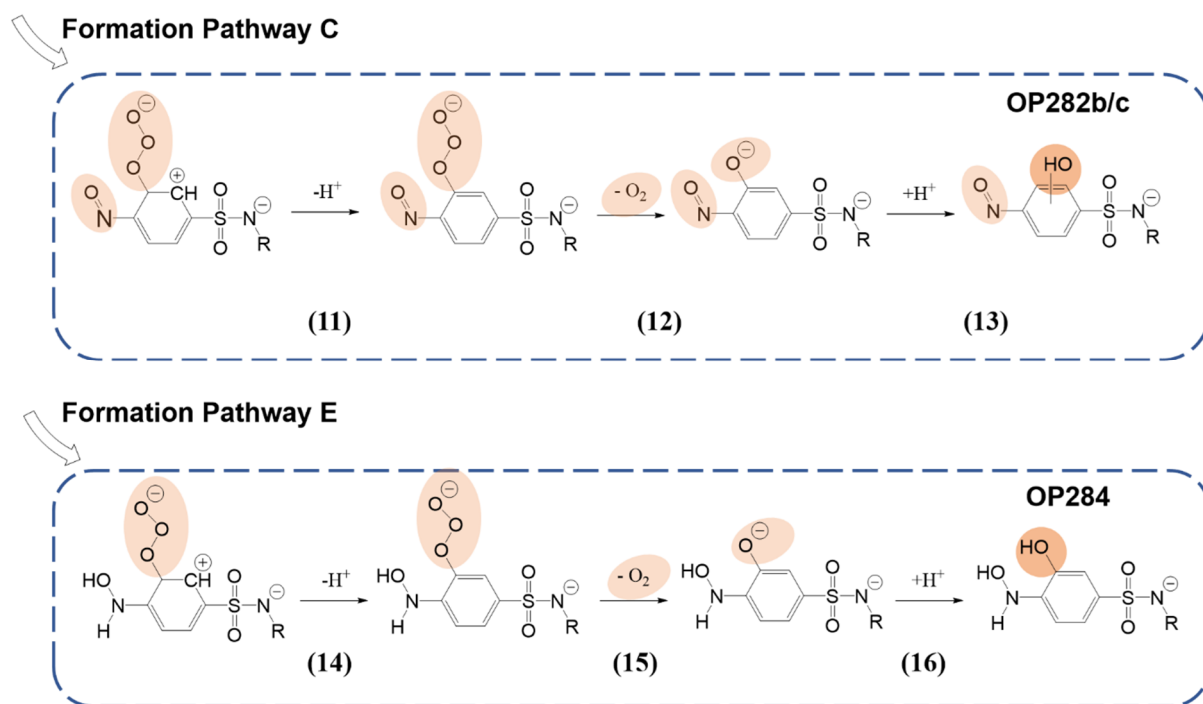


Figure S 9: Proposed reaction mechanism for the formation of OP282 b/c and OP284 in the reaction with ozone. Orange circle highlights the presence of oxygen-18.

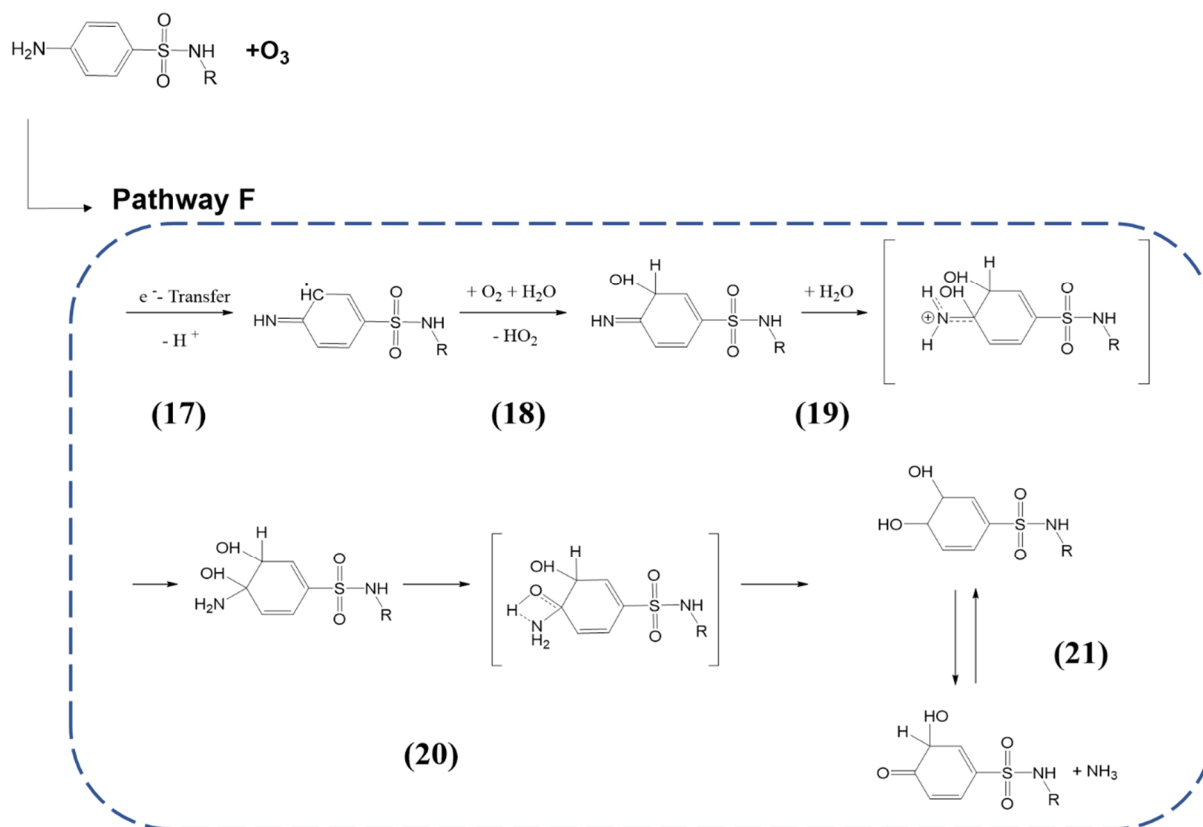
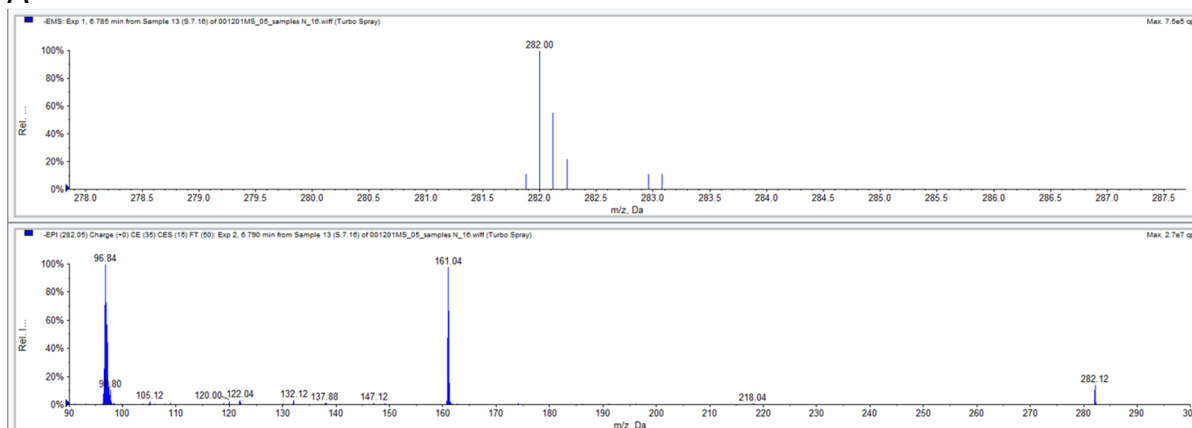
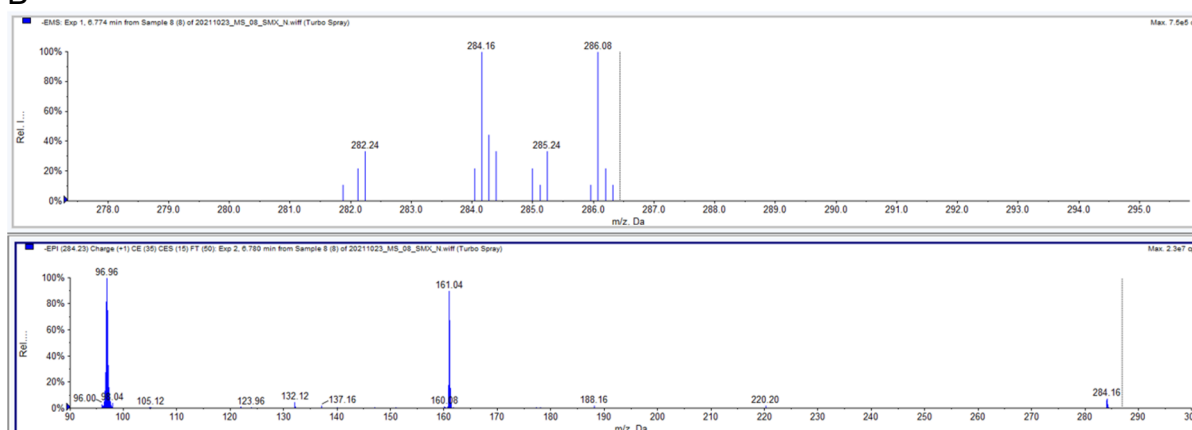


Figure S 10: Proposed reaction mechanism for the formation of OP269 in the reaction with ozone (Extracted from Willach et al. (2017)).

A



B



C

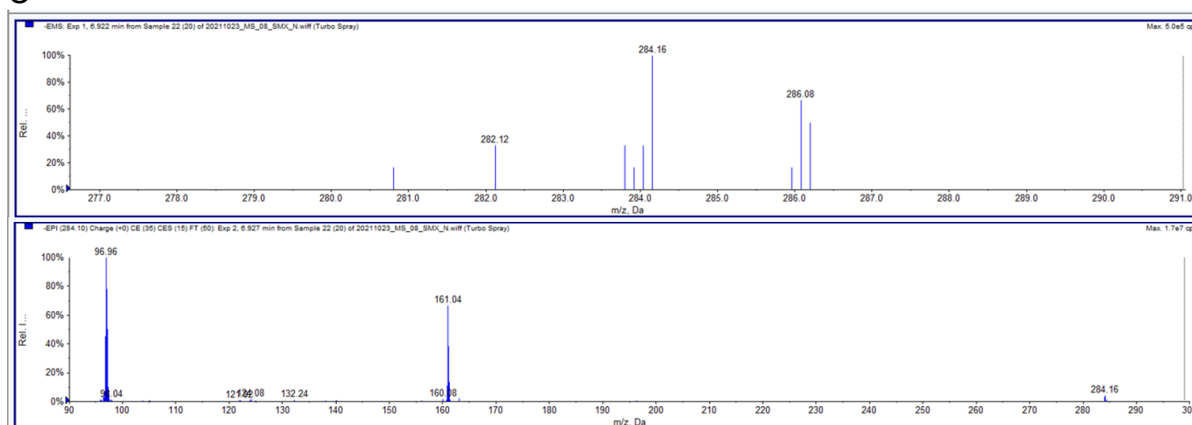
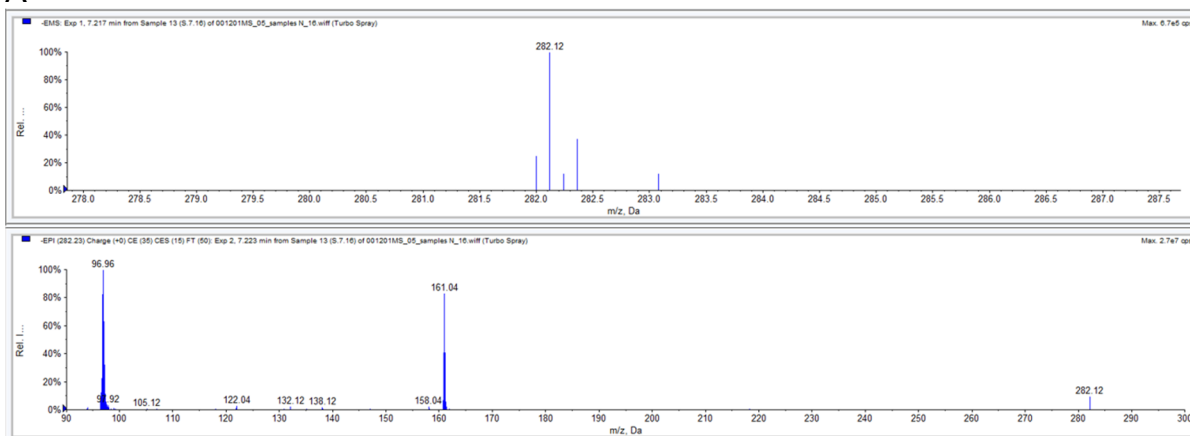
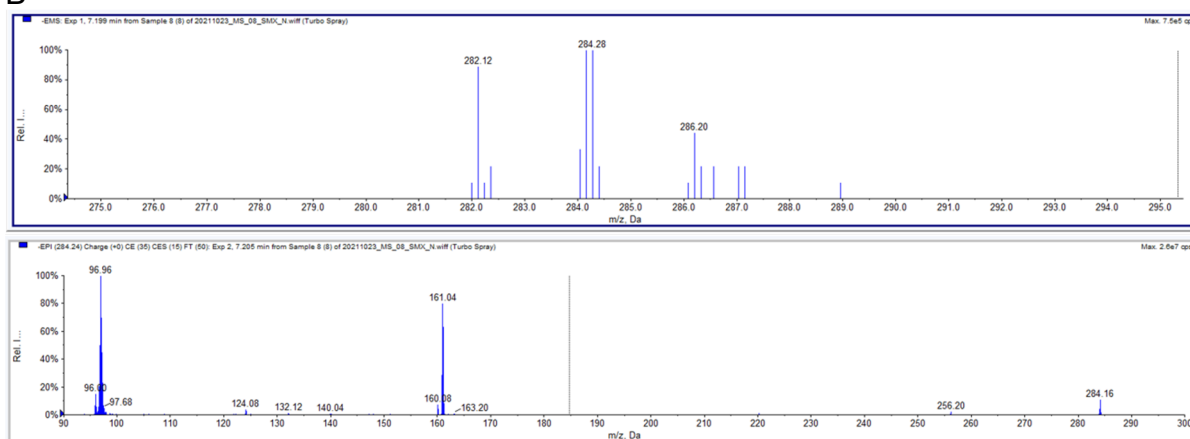


Figure S 11: Fragmentation pattern of OP282b, Rt: 6.7 min. A) ozone produced with technical oxygen ($^{16}\text{O}_2$), B) ozone produced with 55% $^{18}\text{O}_2$, C) ozone produced with 74% $^{18}\text{O}_2$

A



B



C

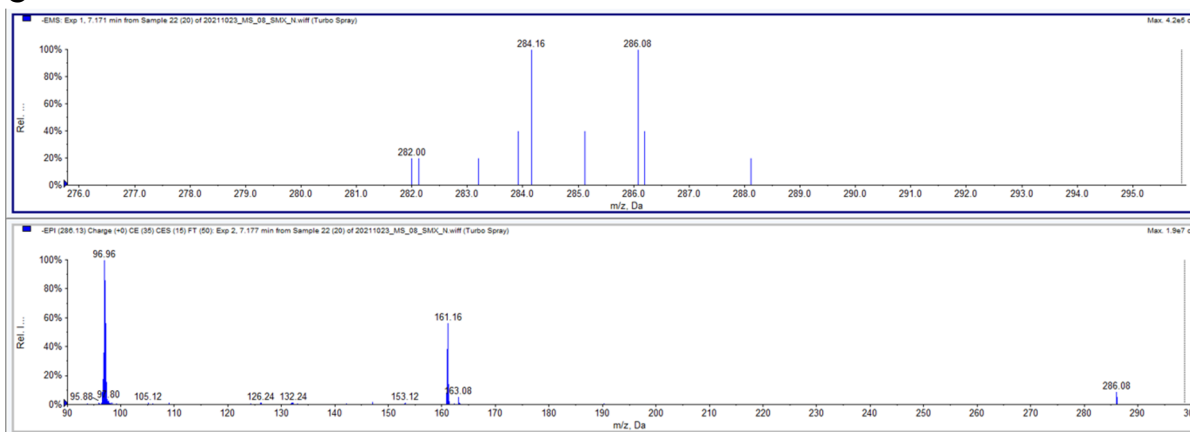


Figure S 12: Fragmentation pattern of OP282c, Rt: 6.7 min. A) ozone produced with technical oxygen ($^{16}\text{O}_2$), B) ozone produced with 55% $^{18}\text{O}_2$, C) ozone produced with 74% $^{18}\text{O}_2$

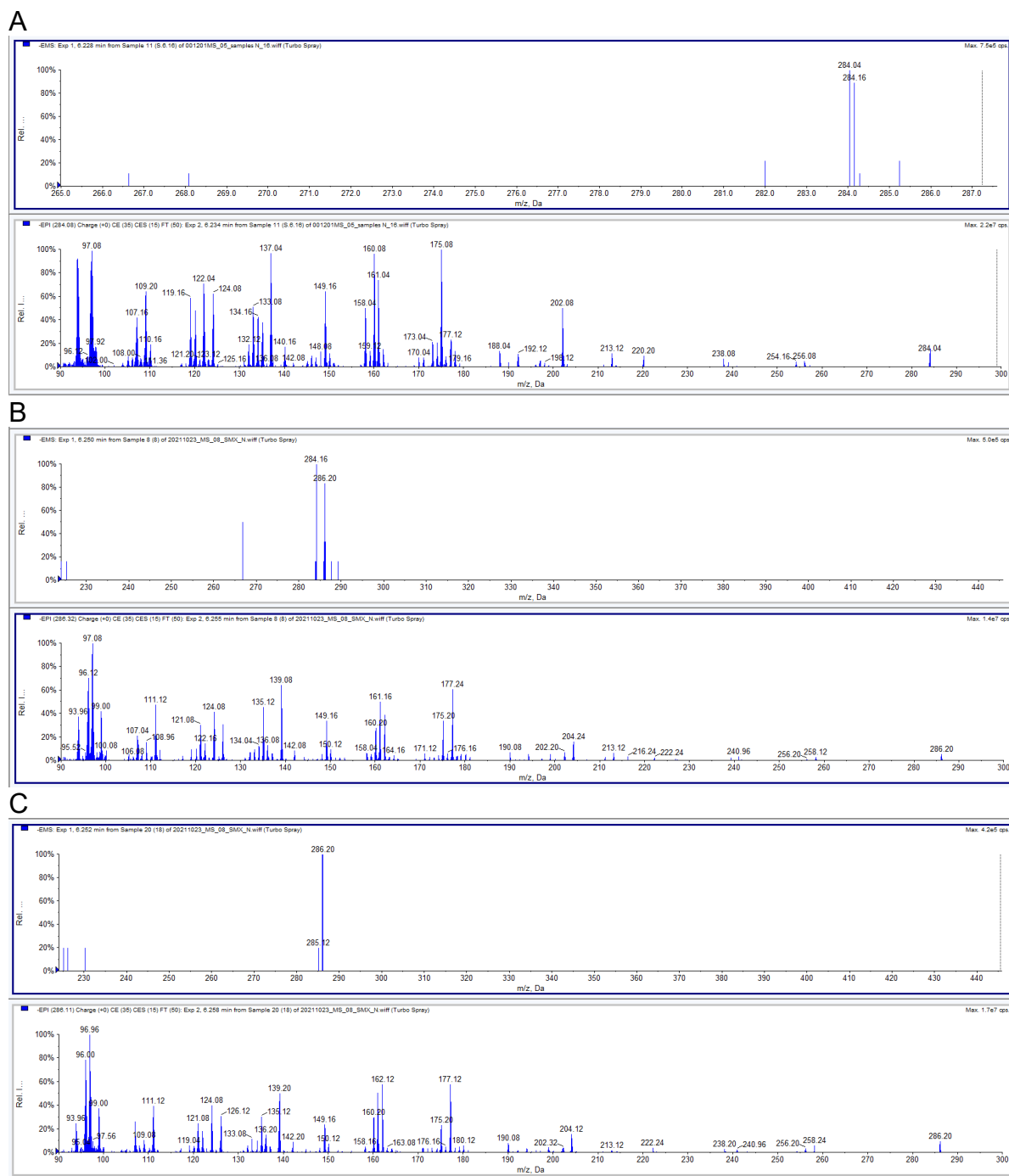


Figure S 13: Fragmentation pattern of OP284, Rt: 6.2 min. A) ozone produced with technical oxygen ($^{16}\text{O}_2$), B) ozone produced with 55% $^{18}\text{O}_2$, C) ozone produced with 74% $^{18}\text{O}_2$